UNIVERSITAT POLITÈCNICA DE VALÈNCIA

UNIVERSITAT POLITÈCNICA DE VALÈNCIA

School of Industrial Engineering

Design of a waveguide-nanoparticle enhanced Raman scattering system for advanced on-chip spectroscopy

End of Degree Project

Bachelor's Degree in Biomedical Engineering

AUTHOR: Arenas Ortega, Daniel

Tutor: Martínez Abietar, Alejandro José

Cotutor: Redolat Querol, Javier Abilio

Cotutor: Pinilla Cienfuegos, Elena

ACADEMIC YEAR: 2022/2023

AGRADECIMIENTOS

En primer lugar, me gustaría agradecer a mi tutor el Prof. Alejandro José Martínez Abietar por darme la oportunidad de poder trabajar en este proyecto en las excelentes instalaciones del Centro de Tecnología Nanofotónica (NTC).

En segundo lugar, dar las gracias al cotutor de este proyecto, el doctorando Javier Abilio Redolat Querol por todas las horas juntos en el laboratorio, por su paciencia para enseñarme todo lo que he aprendido en el laboratorio, por su confianza depositada en mí, por nuestra amistad y por ser tan buen científico como persona.

También agradecer a mi cotutora la investigadora Elena Pinilla Cienfuegos por todo su esfuerzo, paciencia y dedicación por la ciencia, y por su simpatía y alegría que inunda el NTC.

No me voy a poder olvidar de todo el personal doctorando del NTC, gracias por crear un ambiente de trabajo tan agradable.

Agradecer a David Zurita y a Amadeu Griol por encargarse de darnos el material necesario para realizar el trabajo cuando lo necesitábamos.

Por último, aprovecho para dar las gracias a mi Elena por ser el apoyo más cercano que he tenido, gracias por mantenerme cuerdo estos años, te quiero. También a Antonio, a Enrique, a Isa y a las dos Marías por todo este tiempo a vuestro lado. Y a mi familia, que a pesar de estar en otra ciudad me han dado un amor incondicional siempre que lo he necesitado, un beso muy grande.

RESUMEN

El presente trabajo tiene como objetivo la creación de chips fotónicos integrados (PICs) basados en interacción Raman para su uso como biosensores. También tiene como objetivo el montaje de un set-up híbrido para la caracterización de los chips, que combina potenciamiento de la señal Raman con guía de onda (WERS) y con plasmones de superficie localizado (LSP). En el primer capítulo, se hace una introducción del estado del arte, presentando el concepto de radiación Raman, espectroscopía Raman de superficie potencia (SERS) y las consideraciones iniciales para el diseño y montaje del set-up WERS experimental. En el segundo capítulo, se presenta la metodología y materiales utilizados para en primer lugar la funcionalización, transferencia de nanopartículas (NPs) sobre los chips fotónicos y, en segundo lugar, para el montaje del set-up mencionado. El tercer capítulo muestra los resultados obtenidos, donde se muestra la transferencia de nanopartículas en el hueco de dos nano antenas de oro, de dos muestras con diseños diferentes, y su caracterización con microscopía óptica, señales de Raman guiado y en espacio libre. Por otro lado, se presenta la transferencia de nanopartículas sobre un chip con hendiduras de un determinado tamaño que utiliza el efecto de potenciamiento de superficie con plasmón y su señal Raman en espacio libre. A continuación, se muestra el proceso de montaje del set-up, su actual estado y consideraciones finales sobre el mismo. Por último, en el cuarto capítulo, se presentan las conclusiones del trabajo, su impacto y las futuras líneas de avance de este.

Palabras clave: Espectroscopía Raman potenciada con guía de onda (WERS), biosensado, set-up óptico y transferencia de nanopartículas aisladas.

RESUM

El present treball té com a objectiu la creació de xips fotònics integrats (PICs) basats en la interacció Raman per al seu ús com biosensors. També té como a objectiu, el muntatge d'un set-up híbrid per la caracterització dels xips, que combina el potenciament de la senyal Raman amb guia d'ona (WERS) i amb el plasmó de superfície localitzat (LSP). En el primer capítol, es fa una introducció de l'estat de l'art, presentant el concepte de radiació Raman, espectroscòpia Raman potenciada en superfície (SERS) i les consideracions inicials per a el disseny i muntatge d'un set-up WERS experimental. En el segon capítol, es presenta la metodologia i materials utilitzats per a en primer lloc, la funcionalització i transferència de nanopartícules (NPs) sobre els xips fotònics i, en segon lloc, per al muntatge del set-up esmentat. El tercer capítol mostra els resultats obtinguts, on es mostra la transferència de nanopartícules en el buit de dos nano-antenes d'or, de dos xips amb dissenys diferents i la caracterització amb microscòpia òptica, senyals de Raman guiat i en espai lliure. D'altra banda, es presenta la transferència de nanopartícules sobre un xip amb clivelles d'una determinada grandària que utilitza l'efecte de potenciant de superfície amb plasmó la seua senyal Raman en espai lliure. A continuació, es mostra el procés de muntatge del set-up, el seu actual estat i les consideracions finals sobre aquest. En el quart capítol, es presenten les conclusions del treball, el seu impacte i les futures línies d'avanç d'aquest.

Paraules clau: Epectroscopía Raman potenciada amb guia d'ona (WERS), biosensat, set-up òptic i transferència de nanopartícules aïllades.

ABSTRACT

The present work aims at the creation of photonic integrated chips (PICs) based on Raman interaction for use as biosensors. Also, another objective is the assembly of a hybrid set-up for the characterization of the chips, combining waveguide (WERS) and localized surface plasmon (LSP) Raman signal enhancement. The first chapter, an introduction of the state of the art is made, presenting the Raman radiation surface-enhanced Raman spectroscopy (SERS) and preliminary considerations for the design and assembly of an experimental WERS set-up. Chapter 2, the methodology and materials used for firstly the functionalization and transfer of nanoparticles (NPs) on the photonics chips and secondly for the assembly of the mentioned set-up are presented. Then, the third chapter shows the results obtained, the transference of nanoparticles onto the gap of gold nano-antennas of two samples with different designs and the characterization with optical microscope images, guided Raman signals and free space Raman measurements. On the other hand, the transfer of nanoparticles on a chip with slits of a certain size using the surface enhanced effect by plasmon is presented. Then, the assembly process of the WERS set-up, its status, and final considerations about it are shown. In the four chapter, the conclusions of the work, its impact and future lines of progress are presented.

Keywords: Waveguide-Enhanced Raman Spectroscopy (WERS), biosensing, optical set-up and single nanoparticle printing.

INDEX

ACRONYMS LIST

WERS	Waveguide-Enhanced Raman Spectroscopy
BOA	Boosted optical Amplifier
OSA	Optical Signal Analyzer
EDFA	Erbium Doped Fibre Amplifier
PS	Polystyrene
PIC	Photonics Integrated Chip
LOD	Limit of Detection
SERS	Surface-Enhanced Raman Spectroscopy
SPR	Surface Plasmon Resonance
WDM	Wavelength Division Multiplexer
BPT	Biphenyl-4-thiol
AFM	Atomic Force Microscopy
PS	Polystyrene
LSPR	Localized Surface Plasmonic Resonance
NP	Nanoparticle
NPoM	Nanoparticle on Mirror
SAM	Self Assembled Monolayer
IR	Infrared
EM	Electromagnetic

LIST OF FIGURES

LIST OF TABLES

LIST OF EQUATIONS

DISSERTATION

Design of a waveguide-nanoparticle enhanced Raman scattering system for advanced on-chip spectroscopy

CHAPTER 1. INTRODUCTION

1.1. MOTIVATION AND OBJECTIVES

The present work focuses on developing a fully integrated system for measuring guided Raman signals. Wave-guided Enhanced Raman Spectroscopy (WERS) holds significant benefits in various scientific and technological areas. This advanced spectroscopic technique enables improved detection and analysis of molecular vibrations with enhanced sensitivity and precision in comparison with the regular Raman spectroscopy performed in free space. Moreover**, WERS** effectively can be integrated into silicon photonics platforms. Silicon photonics is a well-established technology for on-chip optical devices, making it an ideal platform for integrating WERS. This integration allows for compact, miniaturized, and highly integrated systems, enabling on-chip Raman spectroscopy with improved performance.

WERS achieves high-throughput analysis of samples. By utilizing waveguides and optimized signal coupling, it facilitates efficient light-sample interaction, reducing analysis time as well as non-destructive measurements. This benefit is particularly valuable in applications where rapid and real-time analysis is required, such as in biomedical diagnostics or environmental monitoring. Additionally, WERS can be applied to a wide range of applications in silicon integrating photonics as it allows for the characterization of various materials, including thin films, **nanoparticles** (NPs), biological samples, and chemical compounds. This versatility makes it a valuable tool for researchers and engineers working in different fields, including nanophotonics, materials science, biochemistry, and pharmaceuticals.

Therefore, the current work emerges with the idea of developing a fully integrated system to measure guided Raman signal measurements in on-chip photonic systems, and benefit from all the mentioned capabilities. The work is divided into two main parts. In the first part, two preliminary results are discussed: the transfer of plasmonic nanoparticles onto gold resonance Raman nanostructures by soft-lithography methods and their characterization using a conventional Raman spectroscopy. Nanoparticles are deposited onto the surface of a gold resonance nanostructure; the NP and the gold nanostructure are separated by a molecule's monolayer or a dielectric film. This nanostructure is called in the literature as **nanoparticle on a mirror** (NPoM), indeed, the gold nanostructures used are gold nanoantennaes with a gap of 80 nm length. In the nano-cavity between the NP and the gold surface, the electric field of the electromagnetic (EM) wave is confined and enhanced creating the necessary conditions to measure Raman radiation. The enhancement is produced using the localized surface plasmon resonance (LSPR) phenomena created in the cavity of the NPoM structure.

The second part of the study elaborates on the assembly process for constructing a complete Wave-guided Enhanced Raman Spectroscopy (WERS) **setup**, aimed at enhancing the power coupled into the on-chip photonic circuits based on waveguides and plasmonic (gold) nanostructures. What makes this setup innovative is the absence of any free space components,

thereby minimizing power losses. Additionally, the setup is designed to utilize a beam laser operating at an infrared (IR) wavelength within the range commonly used for telecom applications, specifically λ = 1310 nm. It would be particularly important to perform Raman spectroscopy in this wavelength regime since we may use very advanced equipment (lasers, amplifiers, photodetectors, filters) that have been built to construct high-speed optical fibre networks and systems. The main problem with respect to traditional Raman systems is that the target wavelength is longer, which results in a less efficient Raman process.

Thus, to create a functional Raman biosensor, it is used *Bipheyl-4-Thiol (BPT)* to create a self-assembled monolayer (SAM) of a molecule with a high Raman shift (1/cm). What is more, BPT has a Raman frequency shift that allows to stimulate in the IR band and collect the signal in the visible band, this is known in the literature as **up-conversion**. This phenomenon is already used in the literature for applications in the field of telecommunications, but it can be exploited in biosensing, too. Furthermore, while using our conventional Raman microscope, we are not able to stimulate at the IR wavelengths, the other reason to create an experimental set-up for these measurements.

On the other hand, creating a fully integrated system allows us to create a miniaturized system, which is the first step to create a portable biosensor. Developing a portable device, leads us to create a device which can be used anywhere, with a fast response, low limit of detection (LOD), multianalyte, low cost and high specificity and sensitivity. The device will have applications in the growing sector of the pharmacy, medical diagnostic, environmental monitoring, drug discovery, security, and food quality.

As a far objective of the current work is creating a functional biosensor, **polystyrene** (PS) has been chosen as the analyte to measure the Raman spectra. PS is the perfect analyte for a proof of concept for this Raman interaction biosensor, because its spectrum has a Raman shift in the IR band.

As a previous work, we have the article of J. Redolat [1]. In his work it is assembled the set-up to transfer nanoparticles onto single photonics nanostructures. This set-up it is used to transfer nanoparticles onto the gold nanostructures, used in the sample preparation explained in section *2.5. Lithography method*, subsection *2.5.2 Nanoparticle transfer using* .

This project is part of a final system that will be developed by one of my supervisors Dra Elena Pinilla Cienfuegos, included in a research article presented in the *Fuerzas y Túnel 2023* congress (https://aseva.es/conferences/fuerzas-y-tunel-2023/).

To sum up, the first objective of the current work is transferring nanoparticles onto gold nanostructures for creating a hybrid Raman enhanced photonics chips functionalized biphenyl-4-thiol. Subsequently, the final objective is the design and assembly of a set-up for wave-guided enhanced Raman spectroscopy characterization.

Therefore, to achieve the two main objectives of the work, is necessary to complete a set of specifical objectives indicated hereunder. Moreover, it is indicated the estimated duration of each objective.

- O1: Sample functionalization and nanoparticle transference onto photonics chips.
    - Growing biphenyl-4-thiol SAMs onto photonics chips.
    - Nanoparticle transfer by drop-casting.
    - Nanoparticle transfer by PDMS stamp.
- O2: Structural analysis and functional of gold structures functionalized with BPT and transferred gold spherical nanoparticles (nanoparticle on a mirror structure) onto nitride silicon (SiN_4) substrates.
    - Learning the operation of Raman spectrometer and optical microscope.
    - Learning the operation of *Atomic Force Microscope* (AFM).
    - Structural and functional characterization by SEM, AFM, Optical microscope (MO), conventional Raman spectroscopy and guided Raman spectroscopy.
- O3: Design of WERS experimental set-up.
    - Analysis of WERS set-up implemented in the literature.
    - Free space Raman signal measurement of PS onto a Si-C chip.
    - Study and analysis of the theoretical framework of WERS experimental set-up.
- O4: Assembly of WERS experimental set-up.
    - Assembly and installation of the micro-positioners.
    - Assembly of optical free space elements for input coupling and optimization of the power losses.
    - Assembly of optical elements for output coupling and optimization of the power losses.
    - Assembly of optical elements for measuring guided Raman signal.
    - Guided Raman signal measurement of the functional NP-transferred nanophotonic chip with the WERS experimental set-up.
- O5: Measurements analysis, writing and correction of the dissertation.

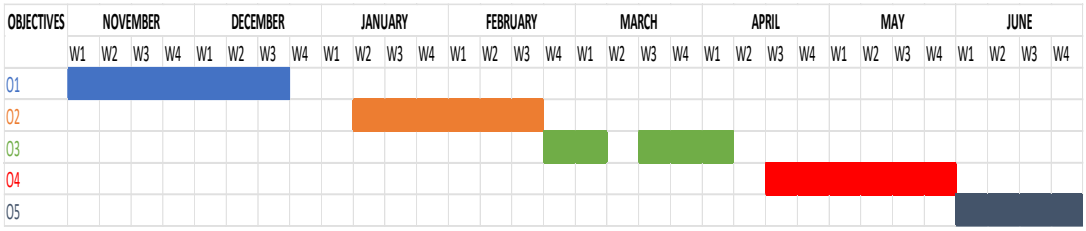

Table 1. Gantt's diagram.

1.2. STATE OF THE ART

The objective of this section is to explain the fundamentals concepts of Raman spectroscopy for biosensing. First, physics basics of Raman dispersion anti-stokes are explained. Then, surface enhanced Raman spectroscopy and waveguide enhanced Raman spectroscopy concepts are explained. Third, practical WERS set-up implementations are mentioned. Finally, biphenyl-4-thiol utility is underlined.

1.2.1. Raman scattering

Raman radiation analyses inelastic dispersion (scattering) of electromagnetic radiation when colliding with a specific molecule. Usually, the incident beam is a laser in the visible or near

infrared (λ = 500 – 800 nm) because molecular vibration frequency is contained in this spectrum, and this cause the Raman resonance phenomena. There are two types of Raman scattering, frequency shift occurs in both. But anti-stokes scattering produces a rise of frequency and stokes scattering produces a loss of frequency. On the other hand, Rayleigh dispersion occurs when incident beam and dispersed beam have the same frequency. Figure 1 illustrates these 3 concepts [2].

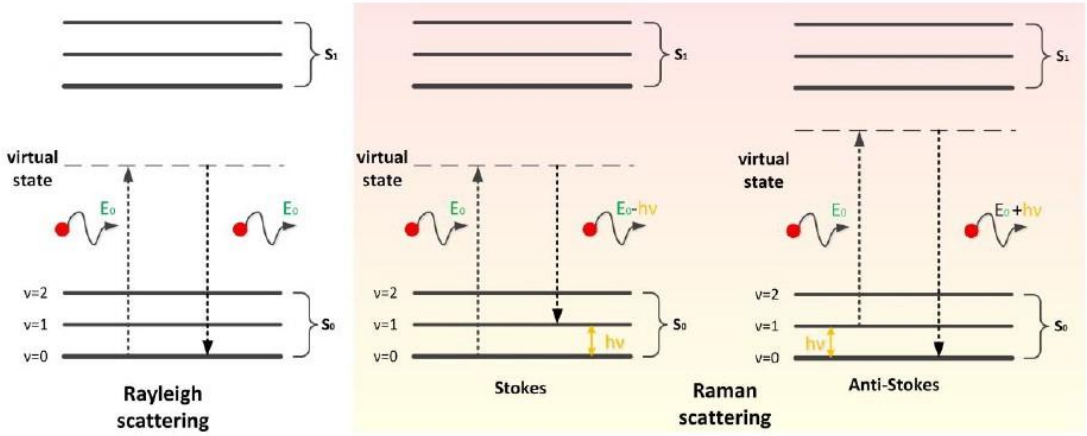

Figure 1. Raman scattering (stokes and anti-stokes) and Rayleigh scattering explained with energy levels (Jablonski diagram) extracted from [2].

Frequency shift is due to the interaction between the incident radiation and the electrons present in the molecule. This interaction consists of an exchange of energy of the radiation to the electrons, which are excited and rise to a higher virtual state of energy. When the excitation is lost, electrons return to his natural state, this phenomenon release energy as a photon with a determinate energy, producing the rise or loss of frequency of the emitted radiation [2].

The resonance frequency vibration of the atom bonds is characteristic of every single molecule. Thus, the frequency spectrum emitted is unique of every single molecule, too. Indeed, it allows to identify the molecule and so, this is the fundamental of Raman spectroscopy [3]. It was modelled by Raman (1928) [4] and equation (1) models the anti-stokes and stokes radiation emitted by the molecule when is excited with an incident electromagnetic beam.

$$\rho = \alpha_0 E_o \cos(2\pi\nu_0 t) + \frac{1}{2}\left(\delta\alpha\delta Q_j\right)Q_{j0}E_o \cos\left(2\pi(\nu_0 + \nu_j)t\right) + \frac{1}{2}\left(\delta\alpha\delta Q_j\right)Q_{j0}E_o \cos\left(2\pi(\nu_0\nu_j)t\right) \quad (1)$$

Where *p* is the dipole generated in the molecule due to the incident electromagnetic radiation, α is the polarizability of the molecule, $E0 \cdot \cos(2\pi\nu 0 t)$ is the electromagnetic field associated to the electromagnetic radiation, Q_{j0} is the amplitude of the normal molecule's vibration mode, $\nu_0 - \nu_j$ is the term associated to the variation of frequency to stokes Raman and $\nu_0 + \nu_j$ the term associated to the variation of frequency to anti-stokes Raman. It must be emphasized that in equation (1) an oscillator electromagnetic field is necessary to generate the dipole emitter of Raman radiation. Indeed, the dipole generates Raman radiation in 3 directions, it beams radiation as a spherical emitter [2].

1.2.2. Raman spectroscopy

In this section is underlined the equation applied to calculate the wavelength associated with the frequency shift of the Raman radiation of the molecule, showed in equation (2). Then, SERS and WERS fundamentals are explained.

$$Raman\ Shift\ (cm^{-1}) = \frac{10^7}{\lambda_{incident}(nm)} - \frac{10^7}{\lambda_{detected}(nm)} \rightarrow$$

$$\lambda_{detected}(nm) = \frac{1}{\frac{1}{\lambda_{incident}} - \frac{Raman\ Shift\ (cm^{-1})}{10^7}} \quad (2)$$

Based on the Raman shift (cm^{-1}) characterized in the state of the art for biosensing molecules, we can calculate the wavelength associated with the Raman signal depending on the wavelength of the incident beam.

To conclude, it must be mentioned that Raman radiation only occurs in 1 photon when 10^7 had collided with the molecule. Thus, enhancement techniques must be used to measure the Raman spectrum of a molecule [5]. SERS and WERS techniques are used to enhance the electric field interacting with the molecule to increase the dipole emitter of Raman signal. Indeed, in this work both techniques are combined to create a hybrid set-up for biosensing applications.

1.2.1.1. Surface Enhanced Raman Spectroscopy in plasmonic substrates

This technique uses the phenomenon of the surface plasmon resonance (SPR), a quasiparticle that is generated on the interface of a metal surface in contact with a dielectric surface when an electromagnetic radiation is applied. A relocation of the molecule's charge of the metal surface occurs, producing an oscillatory electromagnetic field known as plasmon. The enhancement is due to the electromagnetic radiation is coupled to the wave of the plasmon and the electric field increases [6]. For instance, plasmon excitation also happen when a nanoparticle is delivered onto a dielectric surface and excited with an electromagnetic radiation. This is known as Localized Surface Plasmon (LSP) [7]. What is more, in this work nanoparticles are delivered onto plasmonic gold structures functionalized with a BPT self-assembled monolayer. This plasmon technique is known as nanoparticle on a mirror. It enhances the Raman field in a 10^8 factor, but it decreases in 10 to 100 nm [5], the Raman signal can be only measured in the evanescent field region (less than 200 nm).

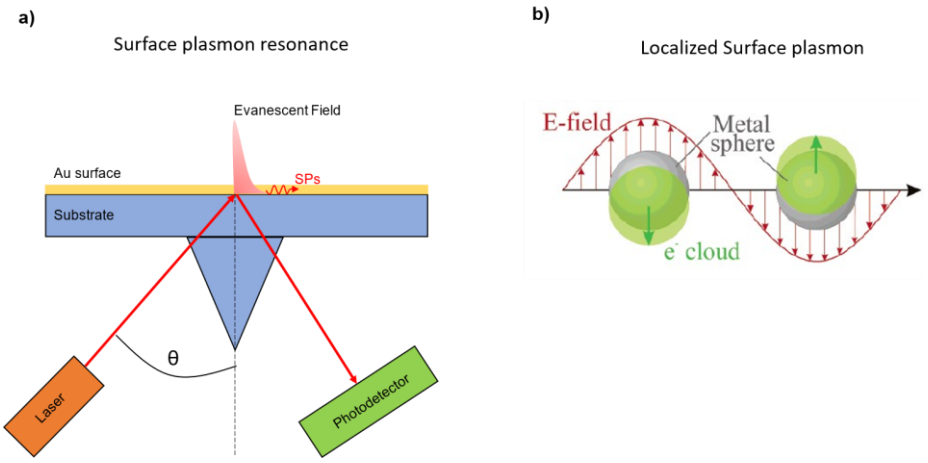

Figure 2. a) Surface plasmon resonance scheme. b) Localized plasmon resonance scheme.

On the other hand, a chemical enhancement emerges, too. It happens due to the bond between the metal and the molecule, enabling the molecule's electrons to new energy states near to the resonance, but this effect only enhances with a 10^2 factor, so it is not too much relevant. But it must be mentioned that molecule's vibration modes influence the enhancement. That means that, the orientation of the molecule is a factor that influences the enhancement. In other words, the polarization of the incident beam and the molecule orientation affects the Raman signal [4].

1.2.1.2 Wave-guided Enhanced Raman Spectroscopy

Recently, it was discovered that Raman active molecules can be stimulated with the evanescent field of an electromagnetic beam coupled into a waveguide [8]. A waveguide is essentially an optical fibre but with a numerical aperture in the scale of nanometres. So, it is made of 2 materials, the cladding with less refractive index (n_1) which is bordering the core with higher refractive index (n_2) such as always is satisfied ($n_1 < n_2$) [9]. For biosensing, waveguide core has two interfaces one with the suspended molecules and one with the cladding Figure 2 illustrates the concept explained.

The slight size of the waveguide (less than 200 nm) allows to couple the light onto it with only one single mode of propagation. Thus, the peak power is not reduced due to modal dispersion and a 10^4 factor of enhanced is reached [5,9].

The measurement of guided Raman spectroscopy implies the design and building of a new set-up. This does not mean that we cannot measure WERS with a conventional Raman spectroscopy system, indeed the spectrums are taken in free space detecting the reflected Raman signal. But, using a specific set-up creates the possibility to reduce the losses, in addition increases functionality, versatility and robustness. In this work, it is presented a WERS set-up that allows to measure Raman signal with 3 types of fully integrated configurations. First, reflection measurements are taken when Raman radiation is measured in the opposite sense of the incident beam, the OF used coupled the incident beam and the collected signal. Second, transmission measurements are taken when Raman radiation is measured in the same sense of the incident beam, a OF couple the incident beam and other OF collect the signal.

Furthermore, transmission measurements can be taken above the sample, indeed must be done in the evanescent field (under 200 nm), one OF couple the incident beam and a cantilever collect the signal. If this is done with a cantilever of a Near-field Scanning Optical Microscope (NSOM), the set-up has the potential to create a light imaging of the sample. Thus, allows to measure Raman in 3 directions of the sample as it showed in Figure 3. Furthermore, a specific set-up for WERS can be combined with SERS nanoparticles to create a hybrid set-up with an enormous enhancement of the Raman signal. The particularity of all these configurations is that the Raman signal is collected and coupled by an optical waveguide. Because of the behaviour of the molecule acting as an emitting source. So, it can be considered as a dipole modelled by equation (4). It can be measured waveguide Raman signal in reflection or in transmission since the intensity of both alternatives theoretically must be equals [10].

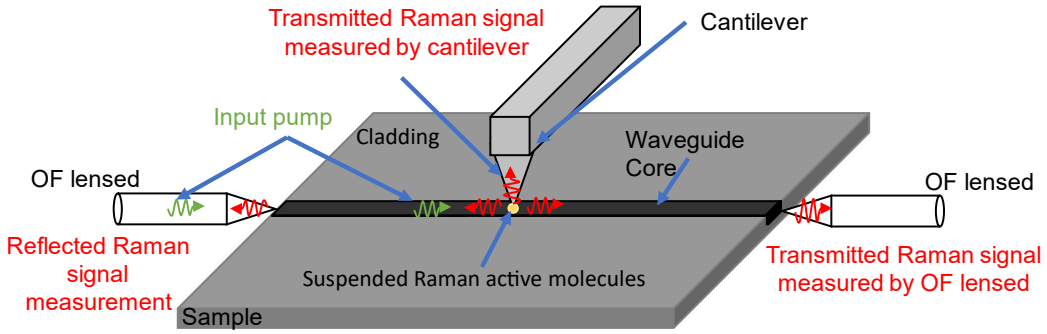

Figure 3. Scheme of the ideal WERS set-up for guided Raman measurements with three configurations: reflection and transmission (above the sample and at the end of the waveguide).

It must be mentioned that several approaches were done in the literature for measuring guided Raman. Articles [11,12] reported the firts measurements. In both articles measurements were done with the collection of the signal with a prism and free space lenses and not fully integrated with optical fibres. But most recent articles of this free space system were done, and it reported that can be improved by creating a fully integrated system [13].

The studies mentioned before having considerable losses due to the free space collection of the signal. So, recently studies try to make it fully integrated with optical fibres. As an example, in [14] it is presented a WERS sensor packed and coupled with a fibre-sample-fibre system.

1.2.3. Wave-guided Enhanced Raman Spectroscopy design considerations

In section *1.2.1. Raman scattering* it was explained the basic theoretical framework of the design of a WERS set-up. The objective of this section is to explain the technical specifications of the design of a WERS set-up.

First, some equations related to the efficiency of the WERS set-up must be used. The equations were modelled by [9] and adapted by [15] and presented here to a further understanding of the critical parameters about the design of the WERS set-up:

1) Raman signal recollection efficiency using Fermi's rule:

$$P_{\omega y}(\bar{r_0}) = p_0 \frac{3n_g}{4\pi}\left(\frac{\lambda_0}{n}\right)^2 \frac{\varepsilon(\bar{r_0})|\vec{d_0}\bar{E}(\bar{r_0})|^2}{\iint \varepsilon_0 \varepsilon(\bar{r})|E(\bar{r})|^2\, d\bar{r}} \quad (3)$$

Where P0 = ω4|d0|/(12π ε0c3) is the irradiated power by the dipole in free space, with a value of d0 , ng is the mode of propagation index, n is the diffraction index, $\varepsilon(\bar{r})$ is the relative permeability, $\vec{d_0}$ is the direction vector of the dipole and E is the electric field. Indeed, equation (3) proves that in high refractive index materials (n) is obtained a higher evanescent field, which creates a higher Raman signal.

2) Dipole emission while excitation by waveguide

$$\left|d_0^2\right| = \frac{\sigma\lambda^4\Sigma^2}{2\pi^2}|E(\bar{r})|^2 \frac{n_g P_{pump}}{\iint \varepsilon_0 \varepsilon(\bar{r})|E(\bar{r})|^2\, d\bar{r}} \quad (4)$$

Equation (4) lecture shows that the square dipole's module ($|d_0|^2$) is proportional to the cross section of the incident beam (σ). It can be expressed as a new equation:

$$\left|d_0^2\right| \alpha\, \sigma \quad (5)$$

The other lecture that equation (4) brings is that in order to enhance the evanescent field of the waveguide, the square of the electric field's module ($|E|^2$) must be maximized, this brings us to evaluate the polarization of the beam. There are two modes of polarization while propagating along the waveguide. First, transversal electric (TE), where the direction of oscillation of the electric field parallel to the chip surface. Secondly, transversal magnetic (TM), whose electric field direction oscillation is orthogonal to the chip surface, as it shown in Figure 4 a) and b). Figure 4 c) demonstrates that TM propagation improves the electric field for a specific size of waveguide, thus a higher evanescent field is interacting with the molecule and using equation (4), it can be determined a higher dipole emission of the Raman signal. So, with these conditions the Raman signal is increased. In this case only is showed for the slab waveguide, but for other geometries the same performance is reported, because the active molecules are always above the sample as it illustrated in Figure 3.

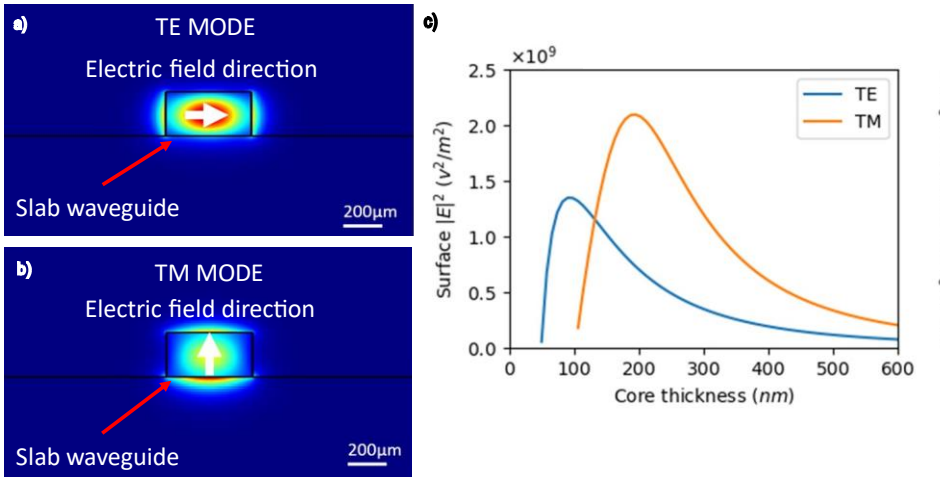

Figure 4. a) Cross section of a slab waveguide with TE mode transmission, white arrow marks electric field direction of the electromagnetic beam b) Cross section of a slab waveguide with TM mode transmission, white arrow marks electric field direction of the electromagnetic beam. c) Relation among the electric field in the surface of the waveguide and the core thickness of the slab waveguide extracted from [5]

3) Relation between waveguide length and power ratio

$$\frac{P_{col}(L)}{P_{in}} = p\sigma\eta_0\gamma_{in}\gamma_{out}e^{-a_pL}L \quad (6)$$

Where P_{col} is the power of the collected signal, P_{in} is the power of the incident beam of the sample, p is the density of the molecule layer above the waveguide, σ the cross section of the waveguide, γ_{in} and γ_{out} the parameters related to the efficiency of the input and output coupled light, respectively. These parameters are determined for a coupling configuration in free space or for coupling with an optical fibre, a_p the losses associated with the length of the beam and L the waveguide length. So, many authors punctuate that waveguides have an optimum length $L_{opt} = 1/a_p$.

To conclude, it must be mentioned that based on the equation showed before, the relevant factors are to a WERS set-up are: 1) wavelength of the incident beam, 2) waveguide materials and 3) waveguide geometry [16].

1.2.3.1 Considerations regarding the wavelength incident beam

As waveguide-enhanced Raman spectroscopy is based in the interaction light-matter, the excitation laser source will have a high influence in the results. Therefore, in this section is underlined the pros and cons of each wavelength band used in biosensing applications, that are directly related with the source selection.

Firstly, the ability to produce laser beam and detect light at a wavelength band is the principal factor to choose a specific wavelength. In other words, the commercial availability of lasers and photodetectors at a specific wavelength. Avoiding this non-technical factor, the parameters evaluated to encourage the efficiency of excitation and recollection of the Raman signal are low fluorescence background noise, low absorption in water (to measure in liquid samples) and low noise Raman. Furthermore, as it shown in equation (5) a higher cross section of the incident beam will make a higher Raman signal, but the relation of the cross section with the wavelength is a factor of λ^{-4}, thus higher wavelengths will produce less Raman effect, for having a low cross section.

To begin with 1550 nm laser band, cross section is highly limited to stimulate the molecule and emit a considerable Raman signal. But this wavelength has the advantage of a low fluorescence noise, low water absorption and great power laser commercially available, due to the number of applications in telecommunications [17].

Secondly, low wavelengths such as 532 nm and 633 nm have a great cross section, hence a great Raman signal. Also, has a great absorption in biomolecules presents in the human body, such as haemoglobin. Low-cost laser and detectors commercially available, too. As a disadvantage, low wavelength has a lot of fluorescence noise in Si_3N_4 y Ta_2O_5 waveguides [2,14].

Thirdly, gold standard for BPT spectroscopy is using NIR laser as input power, 785 nm is the laser used to it. Low fluorescence noise, low water absorption, significant Raman signal are the reason for used it. Otherwise, in biological tissues such as kidney, liver, or lung, it has the inconvenient to has a high fluorescence noise [18].

Finally, using higher NIR wavelengths such as 1088 nm or 1310 nm it is not done yet in the literature. But it presents considerable performance because although it has an inefficient cross

section, the Raman signal losses can be compensated by the higher evanescent field. In Table 2 are summarized all the properties of each wavelength mentioned before.

Wavelength/ Factors	**1550 nm**	**1310 nm /1088 nm**	**785 nm**	**532 nm y 633 nm**
Fluorescence	Low	Low	Low	Very high
Water absorption	Low	Low	Low	Low
Availability of high-power lasers	Yes	Yes	Yes, but there aren't biological tissues that can be stimulated to emit Raman radiation at this wavelength	Low-cost, due to telecom applications
Raman background noise	Great SNR	Not specificized	Not specificized	Low SNR
High Raman signal due to high cross section	Inefficient to Raman	Inefficient but it is compensated with high evanescent field	Reasonable wavelength to stimulate Raman radiation	Less wavelength means higher cross section and Raman signal

Table 2. Determinant factors for each useful wavelength for waveguided Raman spectroscopy.

1.2.3.2 Waveguide materials

Regarding the selected materials for the sample fabrication, it is considered the following aspects.

1. **Refractive index**: High refractive index materials are necessary to get a great evanescent field.
2. **SNR**: A material with low fluorescence must be considered in order to get a better signal-noise ratio and avoid those materials that generate sufficient noise to mask the Raman signal.
3. **Electromagnetic absorption**: Materials with low absorption in the visible and IR band will reduce background Raman noise. Furthermore, a material with an easy microfabrication [19].

Materials that accomplish the requirements are aluminon oxide (Al_2O_3) [20], silicon nitride (Si_3N_4) [21], tantalum pentoxide (Ta_2O_5) [22] and titanium dioxide (TiO_2) [23]. For our samples Si_3N_4 is used because it works perfectly in the visible and telecom wavelengths. Furthermore, NTC microfabrication technical professionals and equipment are configurated to work with it. Also, NTC has developed several projects with silicon nitride and has a properly background knowledge [10,24,25,26].

1.2.3.3 Waveguide geometry

The geometry of the waveguide is a crucial parameter to taking into account because it determines light modes of propagation. Once it is selected the waveguide material, next step is the selection of the geometry. For the current work mono-mode propagation waveguides are integrated with a gold nanoantenna. Therefore, in this section are presented the scheme of 3 basic structures. Figure 5 shows the waveguide designs that are used to create complex designs for biosensing applications.

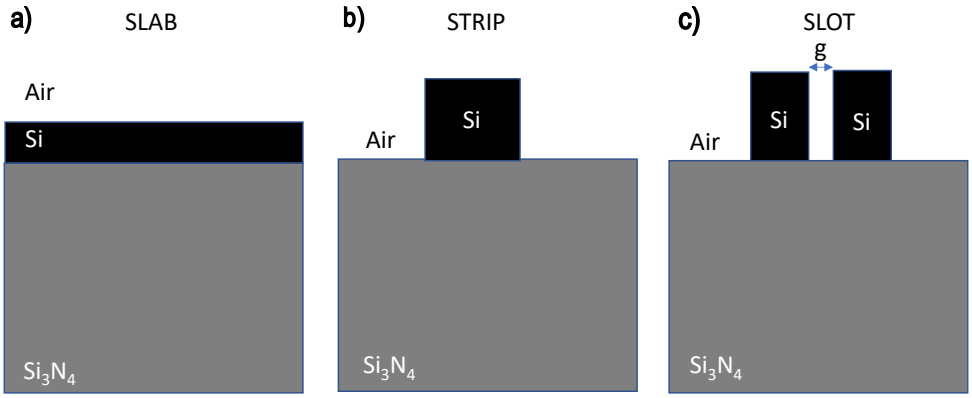

Figure 5. Cross section of a a) Slab waveguide b) Strip waveguide c) Slot waveguide

a) **Slab waveguide**: length and thickness are the relevant parameters. Length is limited by the power loss while interacting with sensed molecules. However, exists an optimum thickness which maximizes the electric field ($|E|^2$). Around this thickness, heavier waveguides will isolate the pump causing a less evanescent field. In the same way, lighter waveguides will isolate less the pump causing more evanescent field [12].

b) **Strip waveguide**: Allows lateral guiding of the pump, but the true advantage is that it can be implemented in a spiral to increase the length for sensing. Using equation (6) can be deduced the optimum length ($L_{opt} = 1/\alpha$). Power losses are minimized with the optimum length [12].

c) **Slot waveguide**: Sensed area has less refractive index than waveguides and is a located between two strip waveguides. Low fluorescence and background Raman noise is obtained with this waveguide because light is confined in "g", which leads to a higher SNR ratio. The confinement of the light is controlled by the width of the slot [12].

1.2.4. Nanoantennae integration

The second part of the work is focused on the study of WERS using integrated plasmonic antennae on a chip. For coupling the Raman signal in a waveguide, we appeal to plasmonic configurations whose design and integration on photonics circuits allows to couple the incident beam, excite the plasmon and guide the Raman signal. A nanophotonic system for extreme confinement and enhancement of light-matter interaction is based on a NP transferred onto the surface of a resonant substrate, this configuration is called nanoparticle on a mirror, as it has been described before. The NP is separated from the plasmonic surface by a mono-molecular layer (NPoM) or by a thin dielectric film. In other words, NPoM is a nanocavity in which the light is highly confined. For our design, NPs and a gold resonator nanoantennae are used because it works well in the band of the wavelength chosen, but other noble metals are used in plasmonic science such as silver or copper [27]. In the present work a molecular nanocavity has been

chosen to create the NPoM structure, for this SAM that must be functionalized, BPT was selected.

Biphenyl-4-thiol is a molecule which can be added in a gold surface as a self-assembled monolayer. BPT Raman spectra has a specific peak in 1585 cm^{-1}, that we called the 1600 cm^{-1} peak, which allows to identify the molecule. As it has mentioned before, this peak appears because the BPT ring vibrational mode is coupled with the incident beam. Figure 6 shows the BPT self-assembled monolayer NPoM Raman spectra [28]. BPT spectrum has two peaks more in 1100 cm^{-1} and 1300 cm^{-1}.

One of the BPT uses is for up-conversion, a process where a molecule is stimulated in the IR or NIR band and the emitted frequency is in the visible spectra, as a consequence of the Raman radiation emitted of the molecule. Thus, this effect is utilized in the literature for telecom and biosensing applications [29, 30].

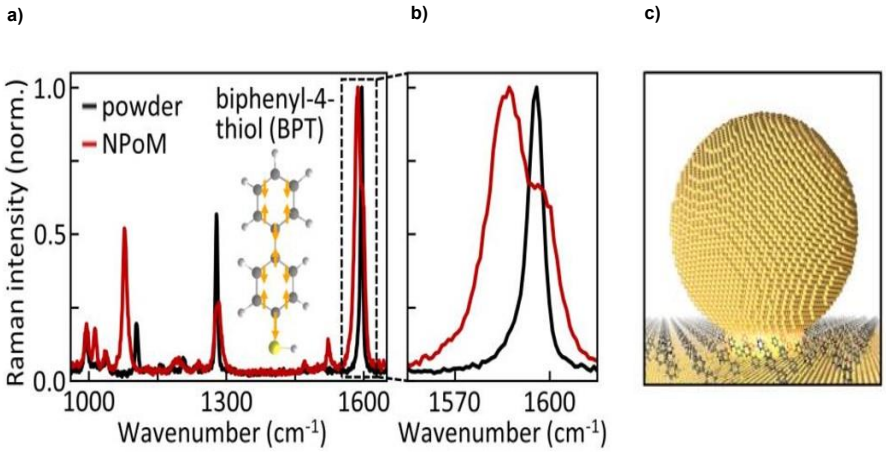

Figure 6. a) Continuous-wave Raman spectrum of BPT powder (black) compared with SERS from BPT in the nanoparticle on a mirror cavity (red). Inset: BPT molecule with arrows indicating the coupled ring vibrational mode (1585 cm^{-1}). b) Detailed view of coupled ring vibration in BP. c) NPoM geometry with molecular layer in gap extracted from [28].

CHAPTER 2. MATERIALS AND METHODOLOGY

2.1. SELECTION OF THE BASIC ELEMENTS OF THE EXPERIMENTAL WERS SET-UP

In the current section are mentioned the materials necessary to build a WERS set-up. First, mechanical materials are mentioned. Secondly, fibre optics utilized are presented. Finally, optical elements are mentioned.

2.1.1 Micro positioners

Micro positioners are commercial mechanical elements meant to place samples or other optical elements in specifics points with a micrometre precision. Its performance is based on mobile platforms that can move in different axes. The micro positioner can be incorporated with a rotation platform on top of the 3D stage. Figure 7 illustrates the 2 micro positioners used in the WERS set-up.

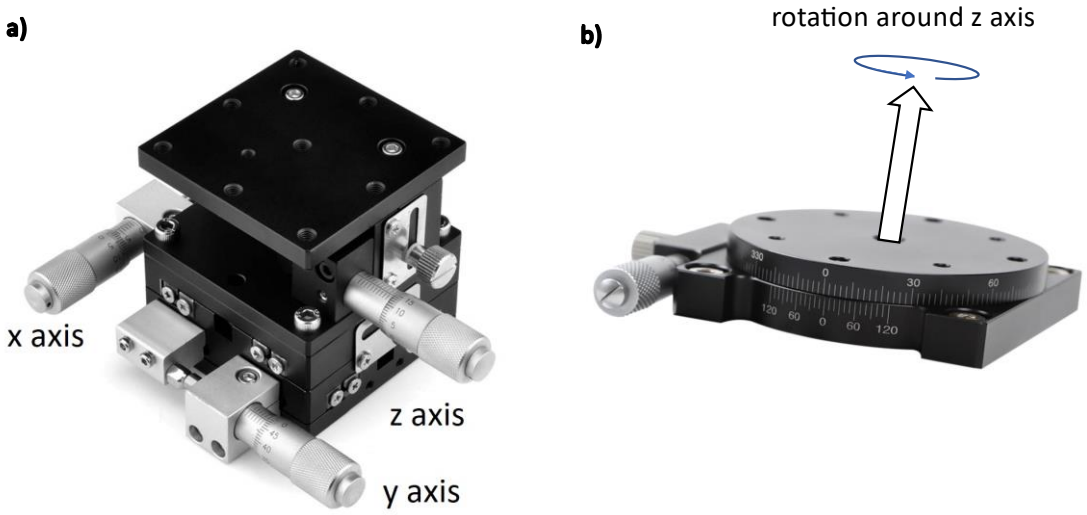

Figure 7. a) Three axes (x, y and z) stage. b) Rotatory (θ) stage.

2.1.2. Optical fibres

For this optical set-up it is used two types of optical fibres. First, to couple light into the sample a lensed optical fibre and cleaved fibre are used. Lensed fibres have an ending tip and allows to couple light into waveguides with more precision and less losses than in free space, Figure 8 b) is a microscope image of the lensed tapered fibre. Furthermore, cleaved fibres are showed in Figure 8 a).

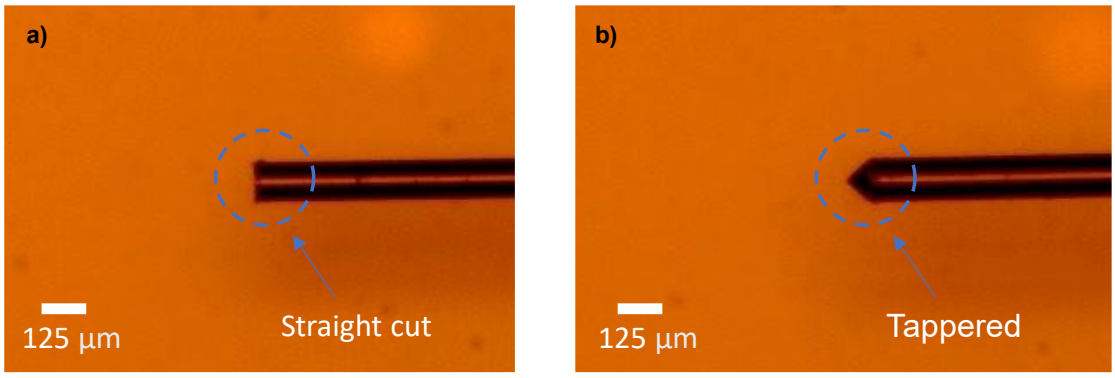

Figure 8. a) Optical microscope image (x20) of a lensed tapered fibre ending. b) Optical microscope image (x20) of a cleaved fibre ending.

The cleaving process was done with a lensed fibre that the tip was broken. Furthermore, it was done with a high precision cleaver, this device can cut the fibre in a straight shape. Indeed, the process of cleaving is illustrated in Figure 9 and explained hereunder. First, remove the buffer of the fibre with some pliers. Then, insert the fibre in the pack and close it likewise Figure 9 b) and c). Next, introduce the pack in the cleaver device. Finally, press the button below and puss down the cover like Figure 9 shows.

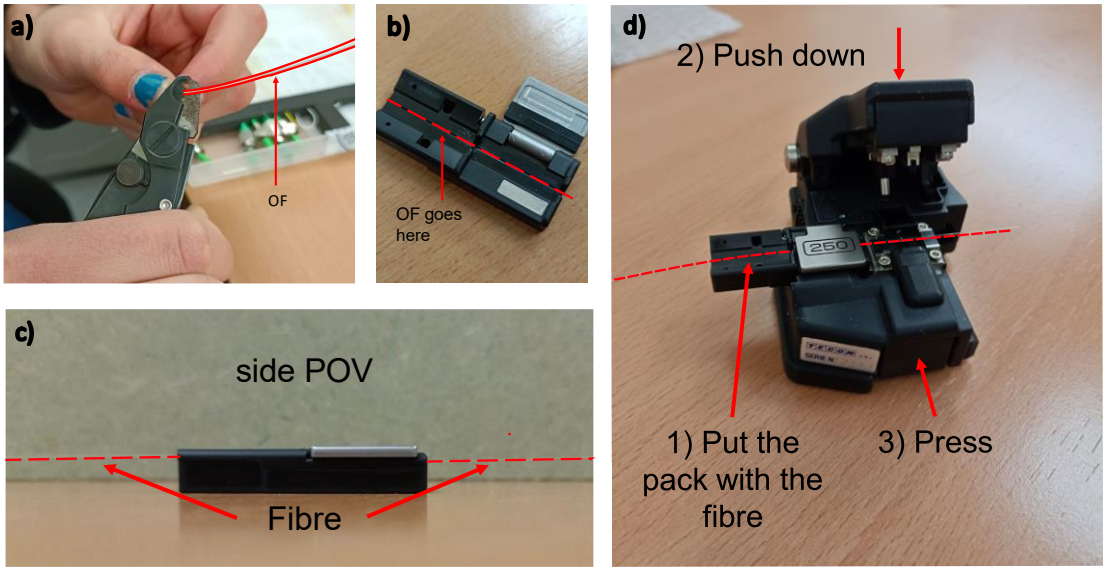

Figure 9. a) Removing the fibre's buffer. b) Cleaver's pack. c) Cleaver's pack side point of view. d) High precision cleaver fully assembly ready to cleave the fibre.

On the other hand, for attaching the lensed fibres to the laser and other optical elements outlined in the next section, two types of fibres connectors are used. The two types of fibre connectors are angled physical contact (APC) and physical contact (PC), both are showed in Figure 10. Fibres connectors PC have a slight bend ending and are connectors simplex multimode, the typical backpropagation loss is – 40 dB. Otherwise, APC connector ends with an 8-degree angle, due to this fact, the reflexion light is backpropagated with a different angle and is not guided backwards. Indeed, this effect increases the backpropagation losses, that are up to -60 dB. APC connectors are simplex mono mode [31].

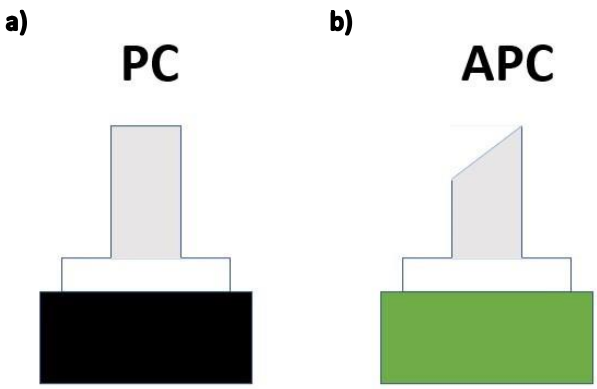

Figure 10. a) Fibre connector PC. b) Fibre connector APC.

2.1.3. Optical elements

In this section is mentioned the optical elements used assembly the WERS experimental set-up. Further details are given in section *3.3. Wave-guided Enhanced Raman Spectroscopy set-up assembly.*

In first place, a tunable semiconductor laser with a regulable wavelength (λ = [1260 nm, 1310 nm]) is used. The laser was used in a specific wavelength and power but, the laser also has a sweep mode, that can sweep a range of wavelengths to take measurements. The laser has a regulable power between -15 dBm and 13 dBm. Furthermore, optical fibre connector with the laser is APC. The laser is shown in Figure 11 a)

Secondly, for the coupling process, it is necessary to have a several number of points of view, in order to couple the fibres and the waveguide. So, two microscopes are used to guide the users to couple the fibres and the waveguides. One microscope is a USB microscope. The USB microscope presents less magnification than conventional microscopes, but it is enough for the purpose in this work. The USB microscope is composed by a lens and a digital sensor that captures the image and transfer it to the computer via USB. The image is displayed in the default camera software that allows the recording of the experiment. The USB microscope utilized is showed in Figure 11 d).

On the other hand, a conventional microscope is placed above the sample to appreciate the lithography properly. The microscope its connected to a camera that can connects via USB with the computer and display real time images. Conventional microscope illumination it is done with an external source supplied by optical fibre. The conventional microscope is showed in Figure 11 b), the camera used is showed in Figure 11 c) and the light source in Figure 11 f).

As we an infrared laser is used, an infrared camera is necessary to couple the laser beam into the waveguide, apart from the two microscopes described before. The infrared camera consists of a matrix of sensors that captures only the incidents photons with a frequency in the IR band. The information received is sent to the computer and displayed on the camera's software. The infrared camera utilized is shown in Figure 11 e).

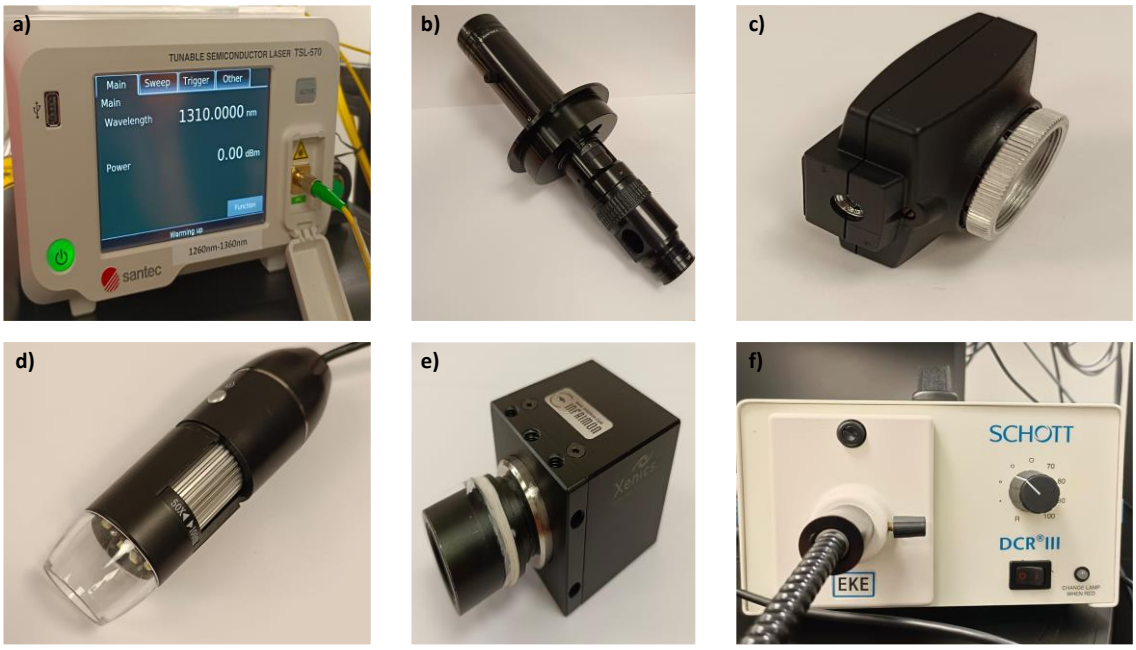

Figure 11. a) Tunable laser. b) Conventional microscope. c) Camera used for the conventional microscope. d) USB microscope. e) Infrared camera. f) Light source

For the preliminary part was used free space parts, in order to couple fibre-sample a collimator (objective) was used. The collimator captures the incident beam and transmits the beam parallel to the ground line. Figure 12 a) illustrates the performance of a collimator, Figure 12 b) shows the real collimator.

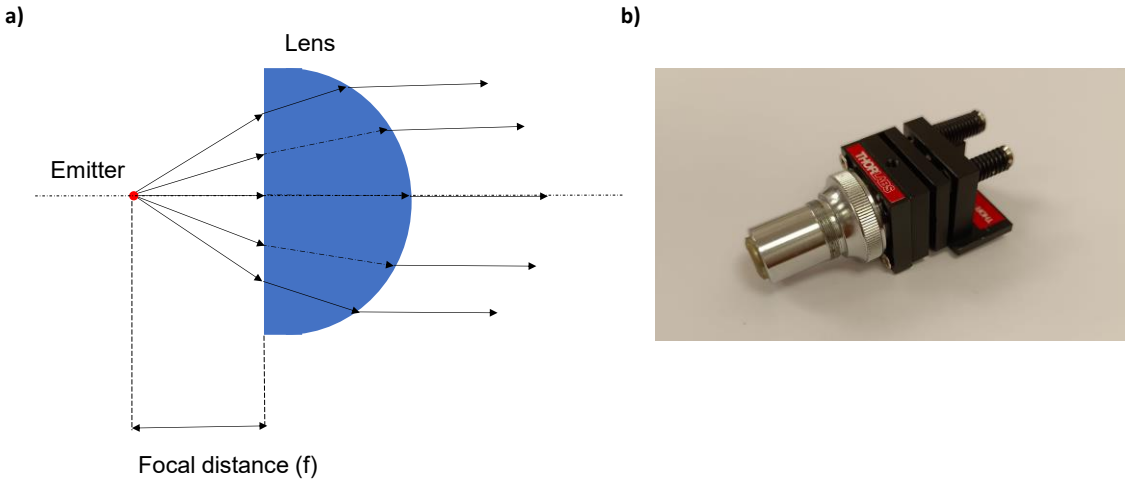

Figure 12. a) Conceptual map of a collimator working as a lens that emit the light beams parallel to the ground line. b) Real collimator.

It is important to be aware that every single part of the set-up can be not working properly. For that, the power meter showed in Figure 13 e) to check the losses (dBm) of each part of the WERS set-up is used. Also, two configurations can be used to measure power or losses with the power meter, Figure 13 d) shows the sensor of the power meter that can be used to measure in free space or integrated.

Still on the theme of checking the power, a visual fault locator was used to check that the components are coupled correctly. Figure 13 b) shows it.

To take guided Raman measurements in the WERS set-up an Optical Signal Analyzer (OSA) is used. The OSA has the resolution enough to measure the incidents photons of the Raman radiation. Furthermore, the OSA performance consists in sweeping the electromagnetic spectrum from 600 nm until 1700 nm with a resolution of 10 pm. It can measure the power in decibel (dB) between -67 db and 67 db with an accuracy of ± 0.4 dB. The optical fibre connector is a straight type (FC) multimode. Figure 13 shows it.

Still on the theme of taking guided Raman measurements, a Booster Optical Amplifier (BOA) was used. The BOA is based in a similar design to Fabry-Perot Laser Diodes. It has an active region made of a semiconductor that creates the light conditions for lasing to occur, but it is used to enhance the intensity of the incident beam. The difference is that BOA's does not have the reflective mirrors to create laser light. As is typical for all amplifiers, BOA's operates in two regimes: a linear and a non-linear, further details of the characterization are given in section *3.3.5. Optical elements for measuring the signal*. Figure 13 c) shows the BOA utilized.

As the amplifier can cause a considerable power of backscattering, an isolator is used to avoid the power backscattered. An isolator is an optical device that only let the light guide in one sense. It is made of a birefringent wedge, which produces that the backscattering electric field and magnetic field diverge. Figure 13 g) shows the isolator used.

As it was mentioned before, the polarization of the electromagnetic field is a key for enhancing the Raman interaction between the beam and the analyte. For that the polarizer showed in Figure 13 f) is used.

Figure 13. a) Optical Signal Analyzer. b) Visual Fault Locator (red laser). c) Booster Optical Amplifier. d) Power meter cap. e) Power meter. f) Polarizer. g) Isolator

2.2. SUBSTRATE FABRICATION

The fabrication process was made by Dr Amadeu Griol, in charge of nanofabrication processes in the NTC facilities. The nanostructure fabrication is divided into several parts explained hereunder:

- **STAGE 1:** The theoretical design of nanostructures. This process was done before this current work, by Javier Redolat the cotutor of this thesis and doctoral candidate, in several projects related to his PhD thesis. In our case, the simulations in CST STUDIO SUITE are used.
- **STAGE 2:** Nanofabrication process technology. To achieve the nanostructure based on the parameters obtained from the simulated structure, there are several steps to follow. In our case, the nanostructures are gold nanoantennae, gold patches and silicon nitride waveguides. Two different substrates were used, quartz and silicon.
    1. **Wafer cleaning.** Starting with a Silicon on Insulator (SOI), whose size can be adapted to the required dimension of the designed substrate. It is necessary an adequate cleaning of the wafer to avoid any errors due to contaminants or moisture during the resin deposition process. Two steps are performed: First, the wafer is cleaned with isopropyl alcohol (IPA) and acetone using the *Coater EVG 101* device, then a plasm oxygen treatment is done with 400 W during 5 to 10 minutes using *Tepla PVA* machine.
    2. **Resin deposition by Spin Coating.** After wafer preparation the resin deposition is done by *Coater EVG 101* machine used before. The objective is to obtain a homogeneous, constant, and defect-free surface using the Sping Coating technique. There are two types of resins:
        - **Positive resins,** whose exposed areas to radiation present inactivated chemical bonds. Therefore, exposed areas will be eliminated from the substrate in the next step.
        - **Negative resins,** whose exposed areas to radiation present stronger chemical bonds. Thus, exposed areas will be conservated from the substrate and radiation-free areas will be eliminated in the next step.
    3. **Aged / Curing.** After resin deposition on the wafer, the solvent is removed to enhance the adhesion between resin and wafer using *Brewer Model 100CB* machine.
    4. **Exposure lithography.** Resin exposition to radiation can be performed through three methods: contact impression, optic lithography, and electron beam lithography (EBeam). In the current work it is used EBeam lithography, where a focused electron beam irradiates the resin. The *Raith 150* device is used for exposure. If irradiating with a negative resin, it must be used a mask with the negative of the desired design. Meanwhile irradiating a positive resin, it must be used a mask with the desired design.
    5. **Developing.** Resin is eliminated from the substrate surface using the *Brewer 100CB* device, the same device used in the aged step. IPA is added to improve the positive resin removal. As it is used a positive resin, the exposed will be removed.

6. **Etching.** Free-resin silicon's wafer is eliminated using the *Reactive Ion Etching with Inductived Coupling Plasma Source (RIEICP)* machine.
7. **Metal evaporation.** Gold nanostructures are transferred to the substrate before the resin is removed. Gold nanostructures such as nano disk, nanoantennae or nano cross also can be also with bottom-up techniques. But in the current work were made by metal evaporation.
8. **Remover.** Last step consists in eliminate the resin used as a mask during the etching step, revealing the final fabricated substrate. shows an illustration of the nanofabrication process technology.

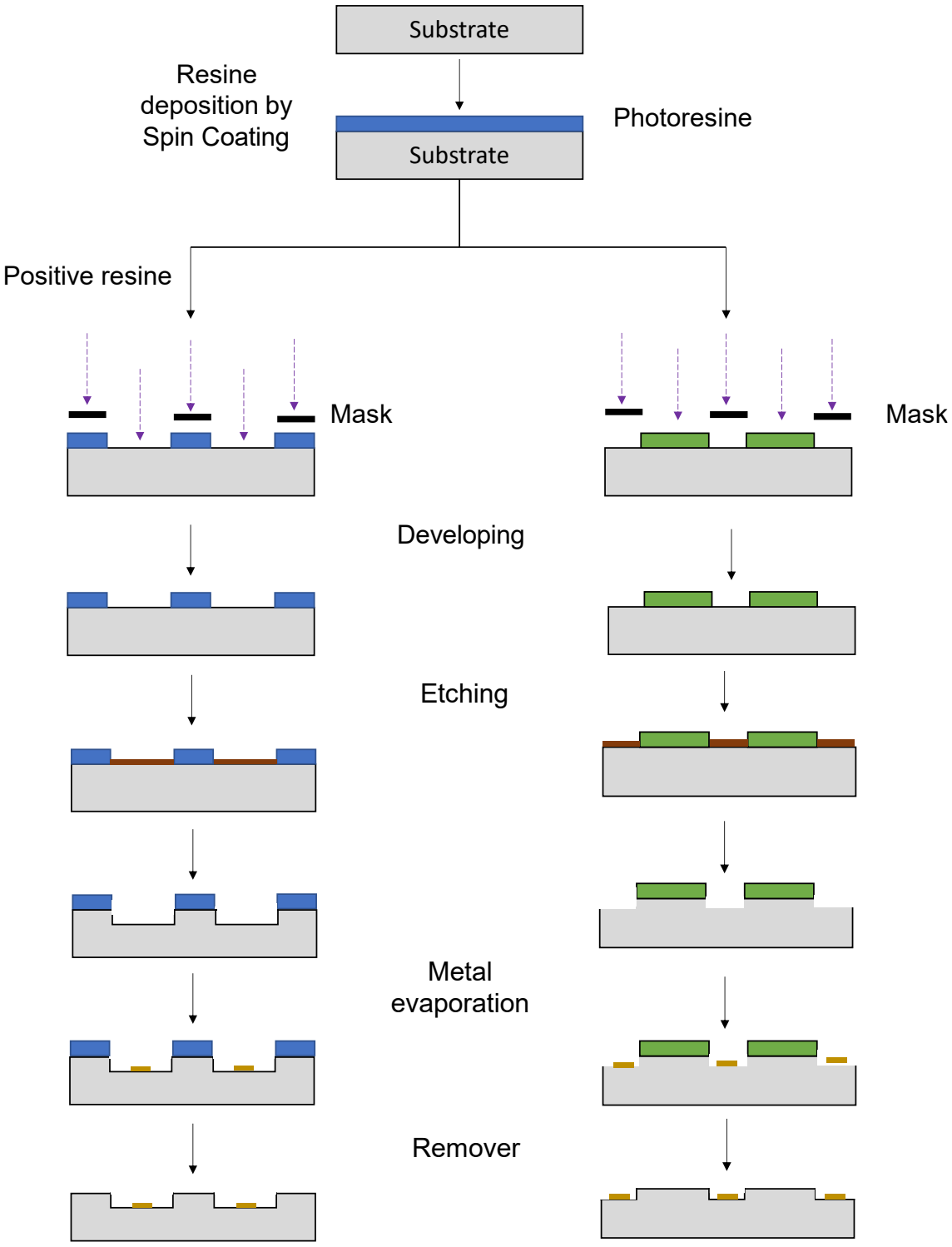

Figure 14. Nanofabrication process to create silicon nitride waveguides and gold nano-antennas.

- **STAGE 3: Wafer inspection and characterization.** Next step is inspection and analysis of possible errors in the nanostructure using the *EBeam* machine or the Scanning Electron Microscope (SEM).

2.3. CHARACTERIZATION TECHNIQUES

2.3.1. Raman spectrometer

For the functional characterization of the gold nanostructures with a nanoparticle transferred onto it, it is used a Raman spectrometer. Also, the equipment has incorporated an optical microscope (OM). Furthermore, the spectrometer features at 532 nm or 633 nm wavelength, whose power can be modulated to 0.1 mW to 26 mW. Furthermore, the polarisation of the beam can be modulated to guide the electromagnetic beam into the waveguide in TM mode or TE mode. The spectrometer collects the reflexion anti-stokes inelastic scattering, obtaining the characteristics peaks of the Raman spectrum of the sensed molecule. These measurements can be in done in a surface using SERS substrates and it can be done in WERS substrates. Figure 15 a) illustrates the process of the conventional Raman spectroscopy measurements.

On the other hand, the process to measure guided Raman radiation is explained and illustrated by Figure 15 b). This is the configuration that it is wanted to improve by the assembly of the set-up. The process is divided in 5 steps. First, put the sample's waveguides vertically attached to a holder with carbon conductive double-side tape. Then, place the sample under the objective and place the USB microscope aligned to see the lithography. Third, focus the sample edge with 10x, 20x, 50x and 100x successively, depending on the roughness of the sample's edge, the focal distance can be variable. Next, place the waveguide under the light of the objective and adjust the focus. Finally, change to the laser configuration and move forward in "x" axis and "y" until the spot is maximized.

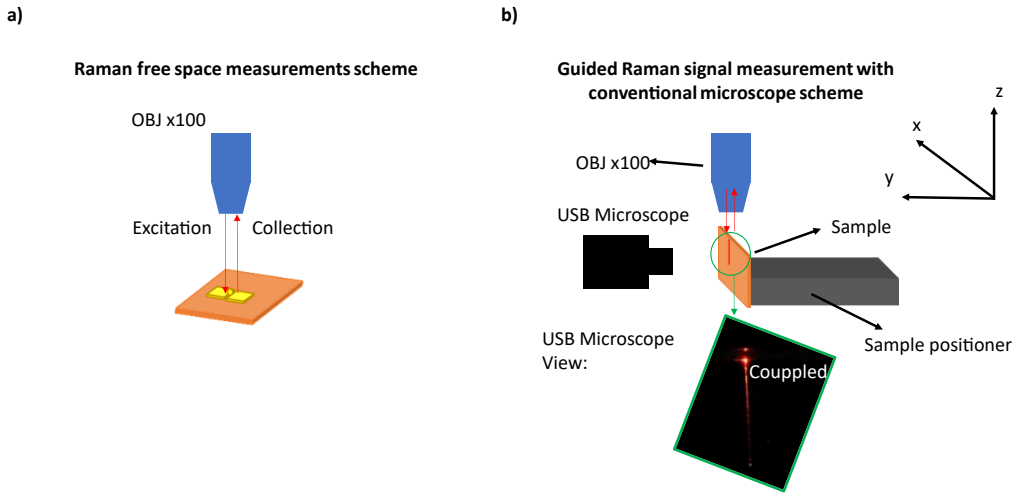

Figure 15. a) Raman free space measurements scheme. b) Set-up for guided Raman measurements with a conventional spectrometer.

2.3.2. Optical microscope (bright field and dark field)

Optical microscope refers to the use of visible light or other forms of electromagnetic radiation in the visible spectrum to observe and study samples at a macroscopic or microscopic level. It involves the utilization of lenses and other optical components to magnify and resolve details of the sample under observation. An image is created by the interaction between light and matter, which is manipulated by the lenses, filters and other devices creating an enlarged and illuminated image of the specimen. This technique enables to study the morphology and structure of the samples, but the resolution is limited by the diffraction limit $\Delta x = \lambda/(2* NA)$,

where Δx is the resolution, λ is the working wavelength and NA is the numeric aperture of the system. There are two common techniques bright and dark field.

2.3.2.1. Bright field (BF)

In BF microscopy sample is illuminated with a bright light source, and the resulting image is formed by the transmitted light that passes through the sample. It was used for the structural inspection and characterization of the WERS and SERS substrates, it is incorporated into the Raman spectrometer for a simply operating. The OM has 10x, 20x, 50x (with two focal distances: 9.1 mm and 0.5 mm) and 100x. The 50x with 9.1 mm of focal distance it was used to illuminate for the side of the sample, to see the scattered light of spherical particles, to easily identify nanoparticles. For instance, BF was used in Figure 24 a).

2.3.2.2. Dark field (DF)

DF microscopy is a variation of bright field microscopy, where the sample is illuminated with an oblique light. It is collected only the scattered light of the different elements of the sample, making visible structures such as nanoparticles against a dark background. The DF optical microscope it is installed in the clean room of the NTC, so it is less accessible than the BF microscope. But it was used to identify nanoparticle transferred into SERS and WERS substrates. The diffracted light of the sample is mostly produced on the spherical nanoparticles. Thus, this phoneme allows to identify nanoparticles easier than using the BF microscope, in samples with a high number of nanostructures. For instance, DF was used in Figure 24 b).

2.3.3. Atomic force microscopy (AFM)

An AFM is a powerful scientific instrument used to study surfaces at the nanoscale level. IT employs a tiny, flexible cantilever with a sharp probe at its tip to scan the surface of a sample. As the probe interacts with the surface, it experiences subtle forces, which are measured by monitoring the deflection of the cantilever. AFM technique enables to cross the diffraction limit that implies the acquisition of high-resolution, three-dimensional image of the surface, even it is possible the manipulation of individual atoms and molecules. The information that AFM images gives; it is the height of the structures with a resolution of nanometres. Furthermore, the AFM characterization that was used the tapping mode, where the cantilever tip is in flickering above the surface at the same time is crossing around it. Indeed, AFM was used to identify nanoparticles transferred onto gold photonics nanostructures.

Hence, in section *2.5. lithography method*, the quartz substrate sample was analysed with AFM, because it cannot be done by scanning electron microscope (SEM). The reason why is because non-conductive samples cannot be measured by SEM.

2.4. BIPHENYL-4-THIOL FUNCTIONALIZATION (BPT)

WERS photonic chips were designed to have a waveguide integrated with a NPoM structure. As it was explained before, in order to create the NPoM structure, a self-assembled monolayer of BPT is necessary to link the NP and the gold nanoantenna. Furthermore, in this nanocavity the electromagnetic field is enhanced, thus integrated Raman signal can be measured. For that, in this section it is explained the methodology followed to grow a BPT SAM on the surface of the photonic chip.

The functionalization process was made following the next steps:

1. Piranha solution (H_2SO_4/H_2O_2, 1:1) was used for beaker cleaning twice.
2. BPT SAMs were prepared by dipping the substrates in 1 mM BPT in ethanol (absolute, reagent grade) for 12 h – 15 h. Times longer than this can create multilayers of BPT.
3. The sample was sonicated in ethanol for 3 minutes, rinsed with ethanol and dried under N_2 stream.

2.5. LITHOGRAPHY METHOD

To create NPoM it is necessary to deliver an individual NP in a specific location. For that, in this section, it is explained the methodology used to transfer a single nanoparticle onto different gold nanostructures previously functionalized. It were used four samples a), b), c) and d) (see Figure 17), in which a nanoantennae was integrated in each design and two types of nanoparticles, ones with 150 nm and the others with 60 nm of diameter (see Figure 16).

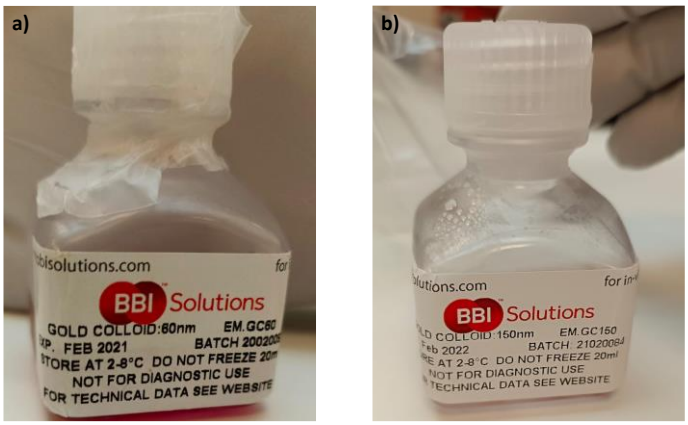

Figure 16. a) Gold spherical colloid nanoparticles with 60 nm of diameter. b) Gold spherical colloid nanoparticles with 150 nm of diameter.

1. **Sample a)**: first waveguide design is a gold nanoantenna attached to a slot waveguide, this sample is designed to measure Raman in reflexion configuration or transmission configuration guiding the light above the sample with a cantilever. But is not designed for transmission configuration with OF. The substrate of this sample is nitride silicon (Si_3N_4). The gold nanoantennae has 80 nm of gap. Each sample contains 7 waveguides separated into 2 groups of waveguides. The sample was transferred with nanoparticles with 150 nm of diameter. Figure 17 a) illustrates the design.
2. **Sample b)**: the waveguide design as a "L" shape, but in the intersection has a gold patch. The gold patch has 60 nm of length. Both waveguides have a slit geometry. The substrate of this sample is nitride silicon (Si_3N_4). Each sample contains 6 waveguides. The sample was transferred with nanoparticles with 60 nm of diameter. Figure 17 b) illustrates the sample.
3. **Sample c):** its waveguide design has a "L" shape, and in the intersection has a gold nanoantenna. The waveguide designed to couple the laser beam has a slot geometry and the waveguide designed to guide the Raman signal in transmission has a slit geometry. The slot geometry facilitates the coupling process because this geometry has a bigger numerical aperture. The gold nanoantennae has 1 µm of length and an 80 nm gap. The substrate of this sample is nitride silicon (Si_3N_4). Each sample contains 7

waveguides. The sample was transferred with nanoparticles with 150 nm of diameter. Figure 17 illustrates the sample.

4. **Sample d):** the sample has several slit waveguides crossing all the sample with a gold patch in the middle. The gold patch has 20 nm of length. This sample is designed to measure Raman signal in transmission configuration. The substrate of this sample is nitride silicon (Si_3N_4). Each sample contains 10 waveguides separated into 2 groups of waveguides. The sample was transferred with nanoparticles with 60 nm of diameter. Figure 17 d) illustrates the design.

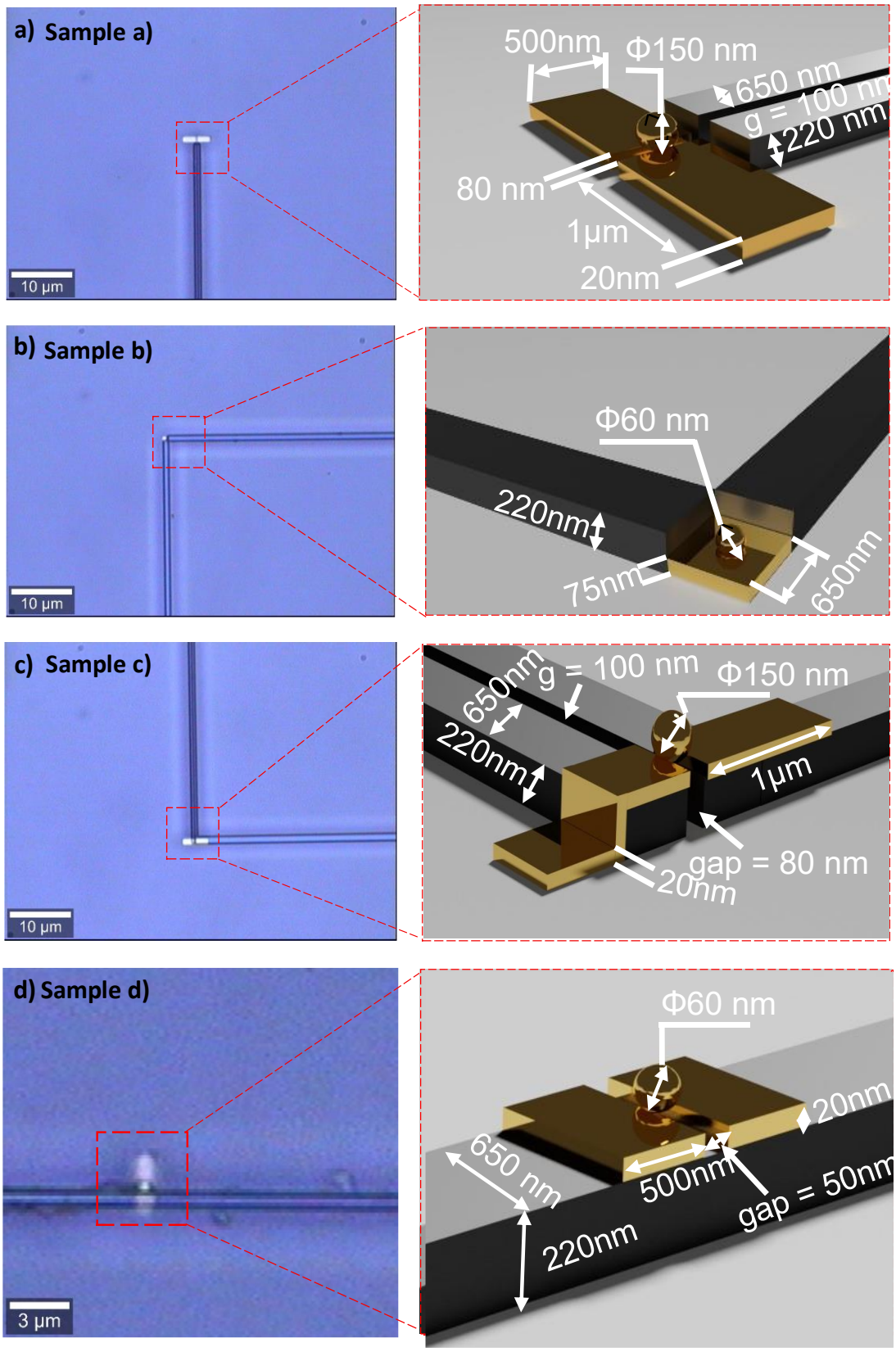

Figure 17. a) Gold nanoantennae attached orthogonally to a slot waveguide. b) Gold patch attached to two slit waveguides with an L shape. c) Gold nanoantennae attached to a slot waveguide and a slit waveguide creating an L shape. d) Gold nanoantennae attached to a transversal waveguide. All waveguides are made of silicon nitride.

Additionally, because of our international collaborations with the University of Cambridge (UCAM) and the École Polytechnique Fédérale de Lausanne (EPFL) it was transferred single NPs on other completely different samples. The sample of EPFL (**sample e)**) consists of an array with several slits with 100 nm width on a silicon substrate, in this case, the NPS must be delivered inside each slit (Figure 18 a)). The slits were used in article [29] for up-conversion process. On the other hand, the sample (**sample f)**) for UCAM consists of an array of two gold patches separated by a nanometric gap (100 nm) on a quartz substrate and the NPs must be positioned in the gap where EM will be confined (Figure 18 b).

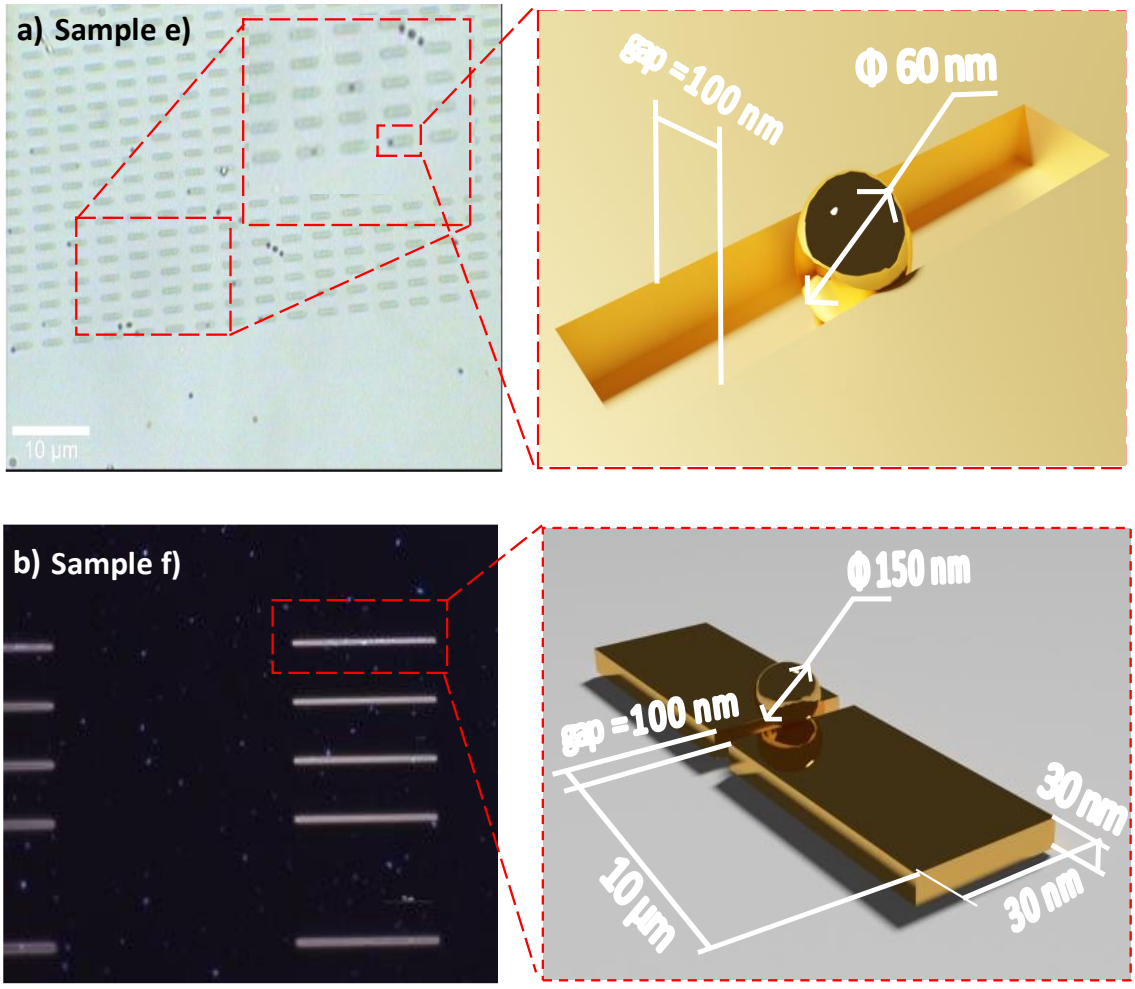

Figure 18. a) Gold slits in silicon substrate used in [29]. b) Gold nanoantennae with 100 nm of gap in quartz substrate

2.5.1 Nanoparticle transfer by drop casting

Drop casting is the most common method to single positioning of NPs onto micro and nano structures. It is a stochastic technique, and the accuracy only depends on probability therefore, the accuracy is shorter than soft-lithography methods. Results will be underlined in the next section, but the yield of this way to NP printing is 1% hence it was utilized an alternative methodology based on soft-lithography using a polymeric material to stamp-assisted the single NP.

However, the methodology of the process to transfer NPs using drop casting is showed below:

First, 10 µL of nanoparticle solution were pipetted and dropped to the samples. Then, waited 30 seconds and rinsed the sample with ultrapure water. Finally, the sample were characterized with the optical microscope, SERS Raman, and guided Raman.

2.5.2 Nanoparticle transfer using soft-lithography

The yield and accuracy of the drop casting method is not so high and to increment the success the process must be repeated it as many times as necessary. Also, for samples with a more complex waveguide design, NP transference can be improved significantly using techniques with polymeric stamps. Soft-lithography methodology was adapted to the samples a) to f) by using two positioning ways: first methodology used was PDMS sweeping and second methodology PDMS stamp transfer.

2.5.2.1. PDMS sweep nanoparticle transfer

This strategy is performed for sample e). It is based on a polymeric mask that brings the NPs above the surface of the sample and the transference is done by the capillary forces between the polymeric mask and the substrate [32,33]. It is used to transfer multiple NPs but modifying the concentration of nanoparticles in each nanostructure to transfer less NPs or even printing a single one. The particularity of this sample design makes this method the most appropriate to print nanoparticles onto its resonant nanostructures.

The sample e) is made of a Si substrate with an array of rectangular holes and gold thin film on top. Then, it was functionalized with a BPT self-assembled monolayer and printed the NPs into each slit. For the last step, it was used a heater (Figure 19 a)), this set-up allows to heat the sample for a temperature from 0 to 120 ºC. Two steps were followed to do the nanoparticles transfer: First, fix the sample to the heater with thermal Scotch tape because it is heat resistant. Second, heat the sample until 100 °C. Then, by drop casting deliver 10 µL of nanoparticles solution. Finally, sweep with a piece of PDMS in the preferent direction of the slits.

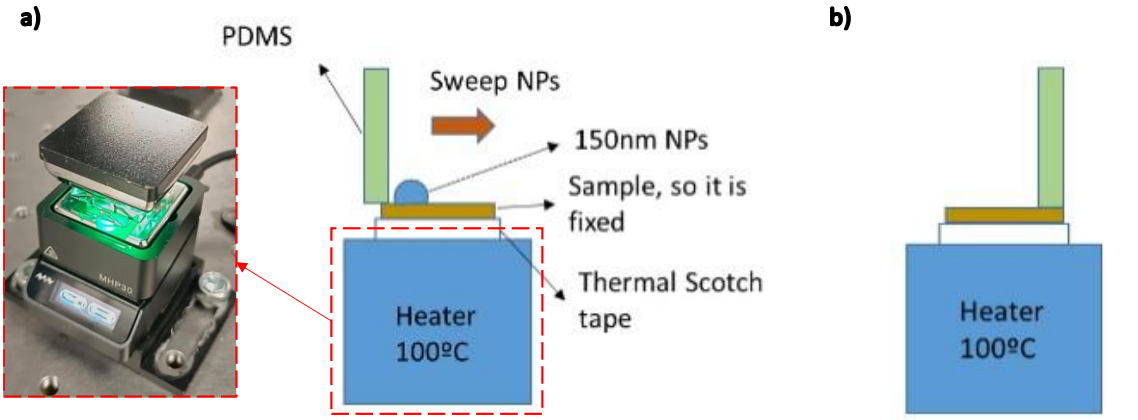

Figure 19. a) Set-up for heating with a precise temperature a sample, first step for transfer nanoparticles by PDMS sweep. b) Second step for transfer nanoparticles by PDMS sweep.

The PDMS elaboration was done using a commercial kit that brings a base and a curling agent. The base and the curling agent were mixed in 10/1 proportion respectively. It is important to stir vigorously because both agents must be mixed perfectly. Some air bubbles can appear due to the stirring phase, as soon as bubbles are notice, sonicate the mix to remove them. Once the

mix was transparent and did not present bubbles, the solution was cured in an oven at 90 ºC for 45 minutes. After this time PDMS was ready for the transfer.

2.5.2.2. PDMS pressure nanoparticle transfer

For more complex samples, in particular, those one which has a nanoantennae integrated with waveguides, it was used a more specific methodology developed for this purpose in a previous work [1]. The set-up used (see scheme in Figure 20) has a 3D stage for the PDMS stamp and a 4D stage for the sample, in order to have degrees of freedom in x, y, z and rotation around z. Rotation around z axis is crucial for the alignment between the sample and the stamp. A rail system is located to move the microscope (O1) placed above the two stages. Also, a USB microscope (O2) was assembled for the manual alignment. A scheme of the set-up is showed in Figure 20 a).

The NP transfer was made following the next steps: First, 20 µL of nanoparticles were delivered by drop casting onto the stamp surface, waited 30 seconds and subsequently remove the overload with a tissue from the side of the stamp (not from the top). Second, place the PDMS stamp on his stage and manual alignment via O1 and O2. Once the stamp is aligned is pressed with a force of 1 N. The process is illustrated in Figure 20 a) to g).

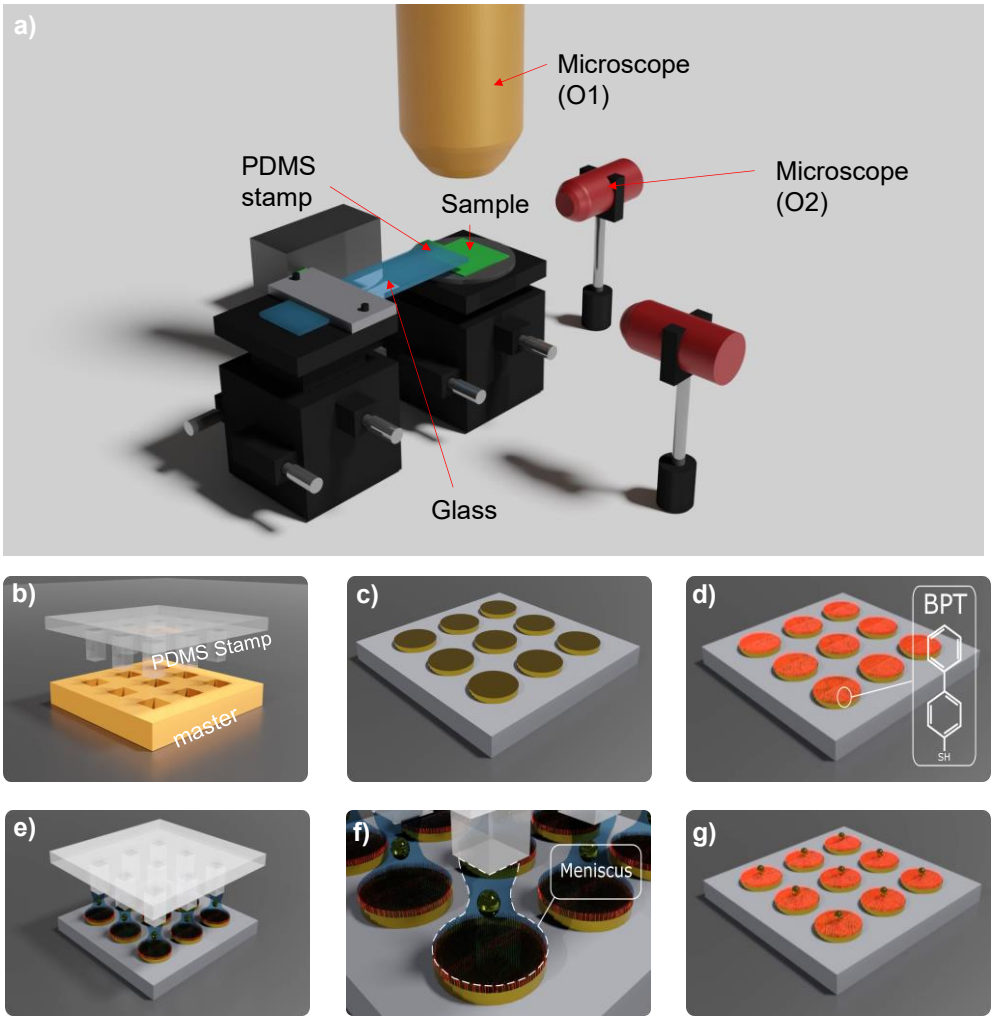

Figure 20. a) Scheme of the transfer set-up. b) PDMS stamp. c) Gold nanodisk.d) Nanodisk with BPT SAM.e) PDMS aligned with the nanodisk. f) Nanoparticle transfer by meniscus formation.gi) Accurate transfer of a single nanoparticle onto the nanodisk

2.6. CHARACTERIZATION OF POLYSTYRENE'S RAMAN SPECTRUM

As a far objective of this work is to create a functional biosensor based on Raman interaction, it was characterised the polystyrene Raman spectrum onto a pure silicon (c-Si) chip. As it was mentioned before, PS has a high intensity peak in 1000 cm^{-1} Raman shift, for that polystyrene was chosen as a good analyte to make the proof of concept. The characterization was done using a conventional Raman spectroscopy and it is necessary to know the expected response of the Raman signal while measuring it with a waveguide integrated Raman spectroscopy.

The followed methodology to characterize the polystyrene Raman spectra has several steps: first, 15 µL of polystyrene was diluted in 8 µL of ultrapure water. Then, a pure silicon substrate (c-Si) was cleaned with isopropanol. Third, 1 µL of diluted polystyrene were delivered onto c-Si by drop-casting.

On the other hand, Raman measurements were taken with 100 magnifications, maximum power, 0.5 integration time, 10 iterations and using wavelength λ = 532 nm. Two measurements were taken, one above the polystyrene and the other above the c-Si.

CHAPTER 3. RESULTS AND DISCUSSION

3.1. CONVENTIONAL GUIDED RAMAN MEASUREMENTS

3.1.1 Nanoparticle deposition with drop casting and BPT Raman spectra measurement

To determine the success of the nanoparticle transference in samples a) and c), several steps were followed: First, samples were analysed with the BF optical microscope to check the gold nano-antennas with a NP transferred into its gap. Then, when it was localized the several nanostructures with NPs, they were characterized with conventional surface enhanced Raman spectroscopy, using 633 nm or 532 nm. Next, on-chip Raman signal was measured with the conventional Raman spectroscopy. SERS and WERS measurements allow to confirm the presence of the NP onto the gold resonance nanostructure, due to, the NPoM nanocavity is assembled correctly, as it enhances the EM radiation making possible to measure Raman signal. If the NP was not delivered correctly, it was not possible to measure Raman signal. Furthermore, the specific Raman shift confirms the presence of a BPT SAM on the sample.

On the other hand, for sample f) DF optical microscope imaging was done to easily identify nanoparticles, due to the DF microscope captures the scattered light. Then, AFM was made to determine the NP transference onto the nano-antennas, because AFM measures the height of the sample and creates a topographic image that can determine the presence of a NP.

To begin with sample a)**,** three attempts were tried to transfer a single nanoparticle onto the 20 nanoantennaes present on the sample and it was only transferred onto four gold nanostructures. In the showed results there are only presented the most accurate NP transferred near the gap, the other 2 NP were transferred too far away from the gap. Thus, it is deduced a low ratio of success and poor accuracy of the method. Furthermore, NP transferred were deposited near the nanoantenna gap, but not in the gap. It cannot be seen in Figure 21 a) and b) but it is deduced it in the guided Raman spectrum, Figure 21 c) and f), because did not reveal the BPT characteristic peaks. However, the NPoM structure works in free space reflexion Raman spectroscopy (SERS) as it showed in Figure 21 b) and e).

To conclude, results do not show the interaction between the beam and the NP when the beam is exciting through the slot waveguide because of the slot waveguide was broken.

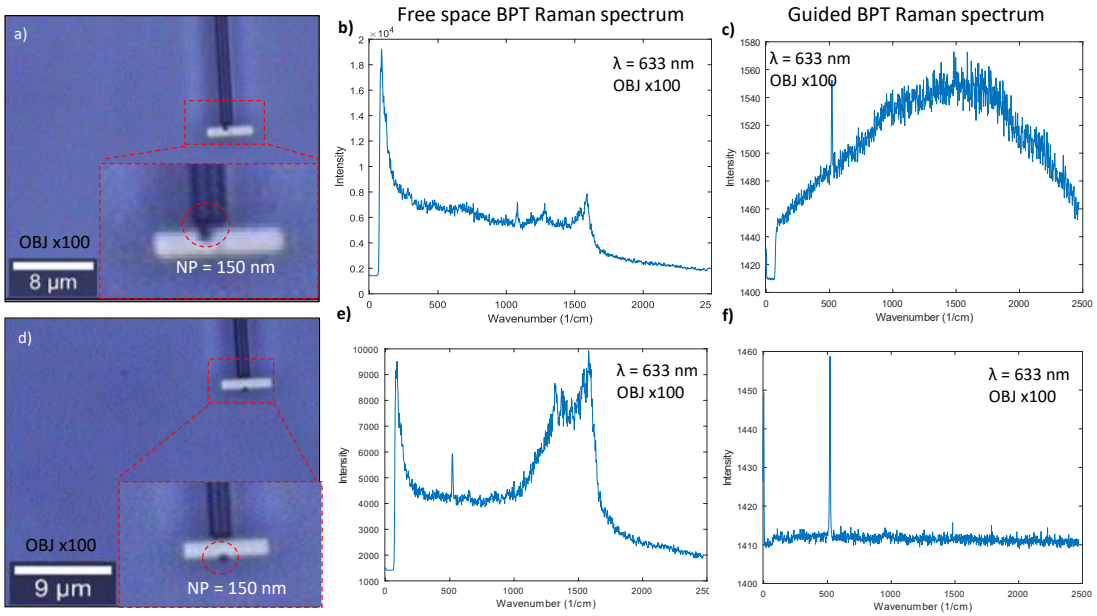

Figure 21. a) Microscope image (x100) of the nanoantenna with a 150 nm particle almost in the nanoantennae gap. b) SERS BPT Raman spectrum. c) Signal measured from the reflexion of the coupled beam. d) Microscope image (x100) of the nanoantenna with a 150 nm particle almost in the nanoantennae gap. e) SERS BPT Raman spectrum. d) Signal measured from the reflexion of the coupled beam.

For sample c) two attempts were committed to transfer NP onto his gold nanostructure. Figure 22 a) and b) shows the result of the second transfer. As we can see, a highly number of nanoparticles were transferred around the nanostructure and waveguides. Two NP was delivered onto the nanoantennae gap showed in Figure 22 a) and b). But only the waveguide b) had a Raman interaction. For the waveguide a), Figure 22 b) shows the Raman mapping of the surface of the gold nanoantennae that was measured. It determines that on the gap, BPT interaction was not find. Figure 22 c) is the free space reflection signal measured using SERS technique and confirms that BPT interaction in this part was not find, too. The non-interaction between the molecule and the electromagnetic field could be for a bad functionalization of the BPT in this gold patch because the Raman mapping shows a BPT response but not the 1600 cm^{-1} peak.

As a result of the NP transferred onto the gap in waveguide b), in Figure 22 c) it is showed the BPT 1600 cm^{-1}, 1300 cm^{-1} and 1100 cm^{-1} characteristics peaks of the guided Raman. The guided Raman was measured by reflection using the red laser and two polarizations, TM is represented in blue and TE mode in orange. TM mode brings a higher intensity of the 1600 cm^{-1} peak. As a consequence of more interaction between the electric field and the molecule. On the other hand, the green laser was used, but a highly fluoresce noise was measured. For both spectrums background was removed (subtraction) and the noise reduced using a median filter.

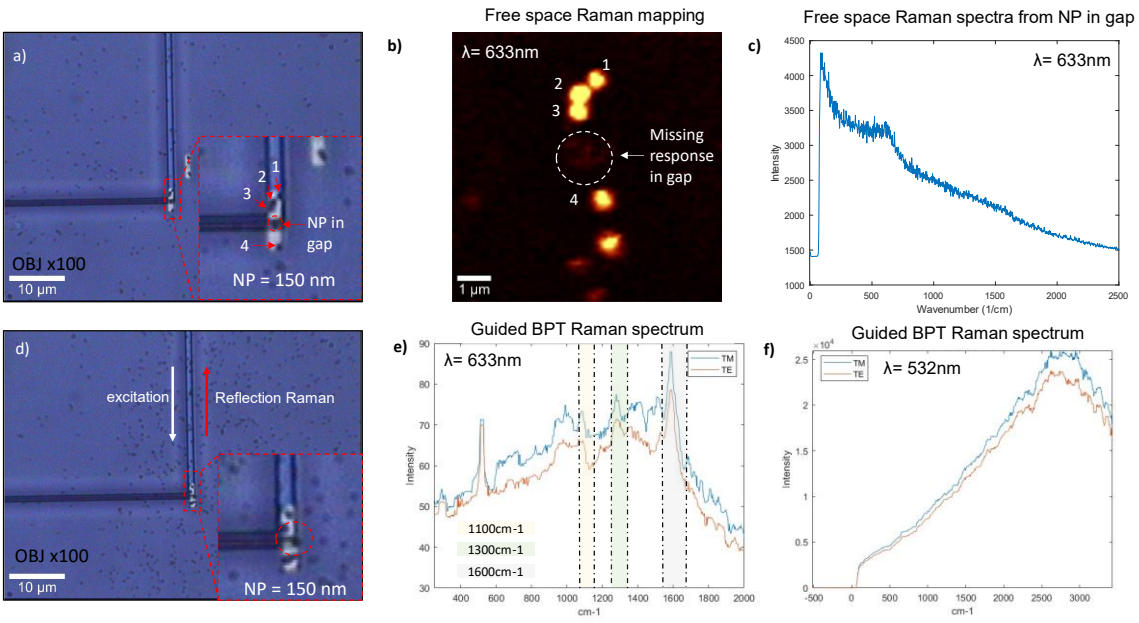

Figure 22. a) Some nanoparticles delivered onto a gold nanoantenna of sample c). b) Some nanoparticles delivered onto a gold nanoantenna of sample c). c) BPT guided Raman from figure b) using slit waveguide and red laser and TM polarization in blue and TE polarization in orange. d) Signal obtained while exciting using slit waveguide and green light

For sample f), using BF microscope in Figure 23 a) and b) it can be seen blue light scattered as it was a spherical gold nanoparticle, but checking with AFM in Figure 23 c), f) and g) it can be seen that there is not any nanoparticle. Also, in these three figures it can be seen a line in the substrate that might be indicating the pull and drag of the nanoparticle. However, Figure 23 d) shows AFM topography of the nanoantennae in Figure 23 e) and it determines that the nanoparticle it is instead a defect of the nanoantennae, that it can be seen underlined in the mentioned figure. Thus, the nanoparticle transfer it must be redone.

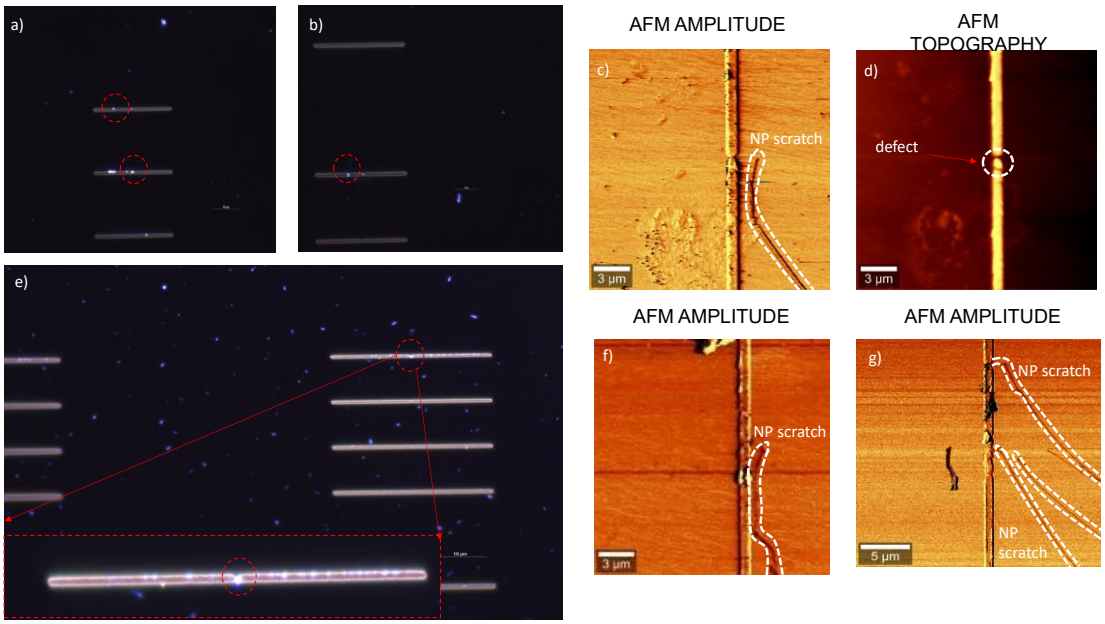

Figure 23. a) Defects on the nanoantennae. b) Nanoparticle transfer onto the nanoantennae but not on the gap. c) AFM amplitude of nanoantennae a). d) AFM topography of the nanoantenna with the defect. e) DF microscope image of the nanoantennae with a potential NP transferred onto the gap. f) AFM amplitude of a nanoantennae of image a). g) AFM amplitude of nanoantennae of image b)

3.1.2 Nanoparticle transfer with PDMS transfer and BPT Raman spectra measurement

Soft-lithography methods were used to improve the accuracy of the NPs printed onto the surface of the gold nanostructures, because soft-lithography it is a specific method to print NPs by reducing the quantity of NPs delivered onto the gold nanostructures. For that, the same as in the previous one, in this section, is presented the accuracy of the method and the characterization using dark field and bright field microscopy images, Raman spectroscopy measurements and integrated on-chip Raman measurements, to determine the correct transference of the nanoparticle in the NPoM structure.

3.1.2.1. Nanoparticle transfer using PDMS sweep

The sample transferred was sample e), the collaboration with the EPFL, the sample with the 100 nm gold slits in a silicon substrate used to up-conversion. Figure 24 a), b) and d) shows that a highly number of nanoparticles were transferred into the slits. In some cases, a dimer of two nanoparticles were delivered. The main characterization technique used was the dark field microscope, it has to be mentioned that as it can be seen in Figure 24 b), nanoparticles have a different colour depending on the dispersion of the colloid size. Furthermore, as the nanoparticles have brilliant colours like blue or yellow, it is easy to identify it in samples with a high number of gold nanostructures such as this sample or sample f). Indeed, using the DF microscope it can be seen the preferent direction of the sweep, which is illustrated in Figure 24 c). Moreover, using SEM microscope allows to see the nanoparticles with more detail, as it can be seen in Figure 24 h), where a dimer of nanoparticles can be appreciated. Indeed, in Figure 24 f) a BPT bridge above the slit.

On the other hand, Figure 24 e) shows the Raman image of the mapped zone of matrix of slits shown in Figure 24 d). Two nanoparticles were selected randomly to see the response to the excitation using λ = 532 nm, by conventional Raman measurement. Figure 24 g) shows the spectrum measured in NP 1, which it can be distinguished the 1600 cm^{-1} characteristic peak of the BPT. Figure 24 i) shows the spectrum measured in NP 2, which it can be distinguished the 1600 cm^{-1} characteristic peak of the BPT, too.

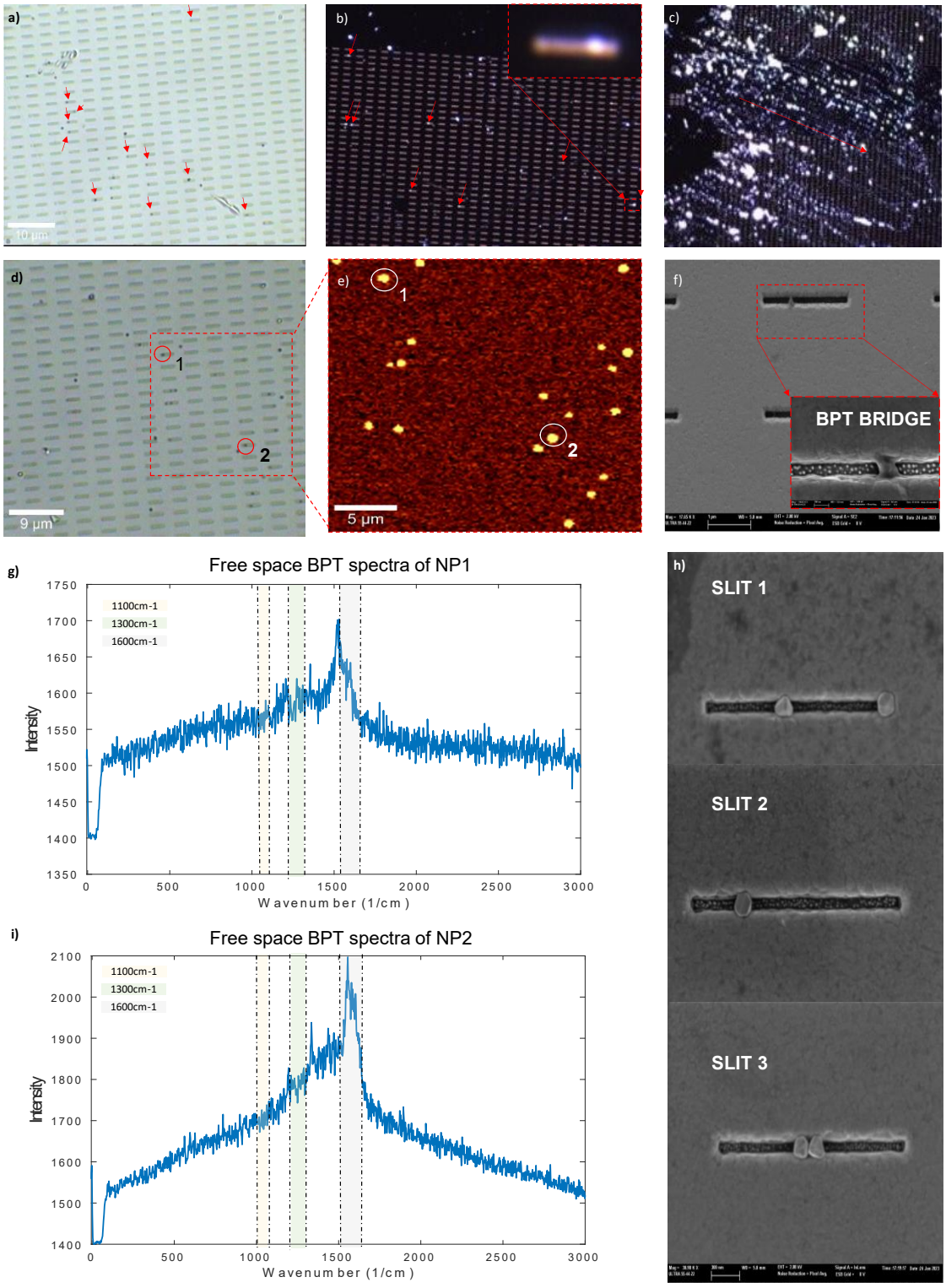

Figure 24. a) Microscope image of one matrix of slits, red arrows highlight the NPs in the slits. b) Dark field image microscope, red arrows highlight NPs in the slits. c) Darkfield microscope image of the preferent direction of the NPs sweep. d) BF Microscope image of one matrix of slits. e) BPT 1600 cm^{-1} Raman imaging of the mapped zone in d). f) SEM image of one slit. g) BPT Reflection Raman spectrum of NP 1 in e). h) SEM image of 3 slits. i) BPT Reflection Raman spectrum of NP 2 in e).

3.1.2.1. Nanoparticle transfer using PDMS pressure

For this part, sample a) was used. This sample was the one with a nanoantennae with a 80 nm gap integrated with a slot waveguide for reflexion measurements. One attempt was necessary

to transfer simultaneously 5 nanoparticles onto the gold nanoantennae, out of a total of 20 nano antennas, as it showed in Figure 25 b). This leads, to a better ratio of accuracy than using drop casting. For one of them the NP was transferred in the gap, as it showed in Figure 25 c). The BPT guided Raman spectra measured by coupling the red laser into the slot waveguide is showed in Figure 25 b). Two polarizations were used TM (blue) and TE (orange), because of a better interaction between the electric field and the molecule the medium intensity of the Raman radiation is higher using TM than TE. About the guided Raman spectra of BPT, it must be underlined that the 1600 cm^{-1} and 1300 cm^{-1} can be observed in the spectra, but the 1100 cm^{-1} cannot be seen.

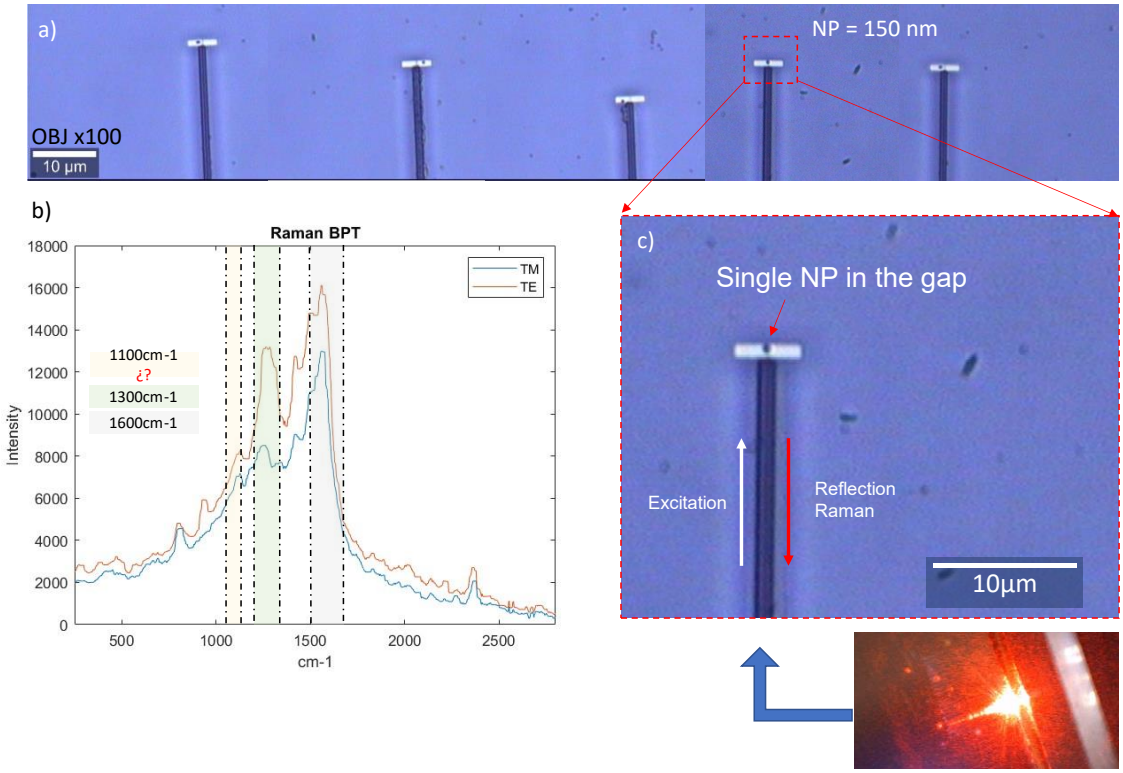

Figure 25. a) Five gold nanoantennae with a NP transferred onto it. b) BPT guided Raman spectrum measured with λ = 633 nm and TM polarization (blue) and TE polarization (orange). c) Single NP transferred in the gap and a real image of the set-up with the red laser coupled to the waveguide.

3.3. WAVE-GUIDED ENHANCED RAMAN SPECTROSCOPY SET-UP ASSEMBLY

This section has two different objectives, first determine silicon wavelength shift of his Raman anti-stokes scattering while exciting with λ = 1310 nm. Then, measure polystyrene Raman shift and calculate the wavelength shift of his Raman anti-stokes while exciting with λ = 1310 nm. This step is made because two main reasons: first, because as a further objective of this work is to create a functional biosensor, PS was chosen as the analyte due to its high Raman shift at 1000 cm^{-1}. Secondly, the other reason is because, Raman shift is necessary to confirm that the WERS is working well when it is assembled. In other words, silicon Raman peak is going to be use as a proof of concept that the WERS can measure on-chip Raman signal. The second objective is to explain the **elements** used to assembly the WERS set-up and the **coupling** process of the input and output OF to the sample. The WERS experimental set-up as it has mentioned before, it is assembled because it is going to be a fully integrated system to measure on-chip Raman signal.

As a fully integrated system, it will reduce the losses due to free space parts and will allow exciting at an IR wavelength. Furthermore, it will be incorporated a NSOM head with a cantilever to create light images of the sample. Moreover, the WERS experimental set-up is the first part to create a miniaturized device that can be implemented as a portable biosensor.

For the design of the set-up, the work has been divided in four parts. The first part is the input fibre assembly and coupling process. The second part is the power optimization of the light coupled to the waveguide. Third part is the output fibre installation and coupling process. Finally, the last part is the assembly of the elements necessary to amplify and filter the Raman signal.

In first place, it must be mentioned that the optical set-up was mounted on an optical bank because is necessary to align the optical elements. Furthermore, the optical bank has an electromagnetic radiation isolator, due to is surrounded by a Faraday's cage. The Faraday's cage is necessary to create light images of the sample using the NSOM.

3.3.1. Polystyrene Raman peak measurement

For the results Figure 26 a) shows the pure silicon (c-Si) spectrum, where it can be noticed the well-defined peak in 521 cm^{-1}. Figure 26 b) shows PS spectra, where it can be noticed the well-defined peak in 1000 cm^{-1}. Figure 26 c) shows both peaks together. It has to be mentioned that c-Si does not hide the PS 1000 cm^{-1} peak. Thus, polystyrene Raman spectra can be measured using the WERS experimental set-up or other Raman biosensor developed in the future.

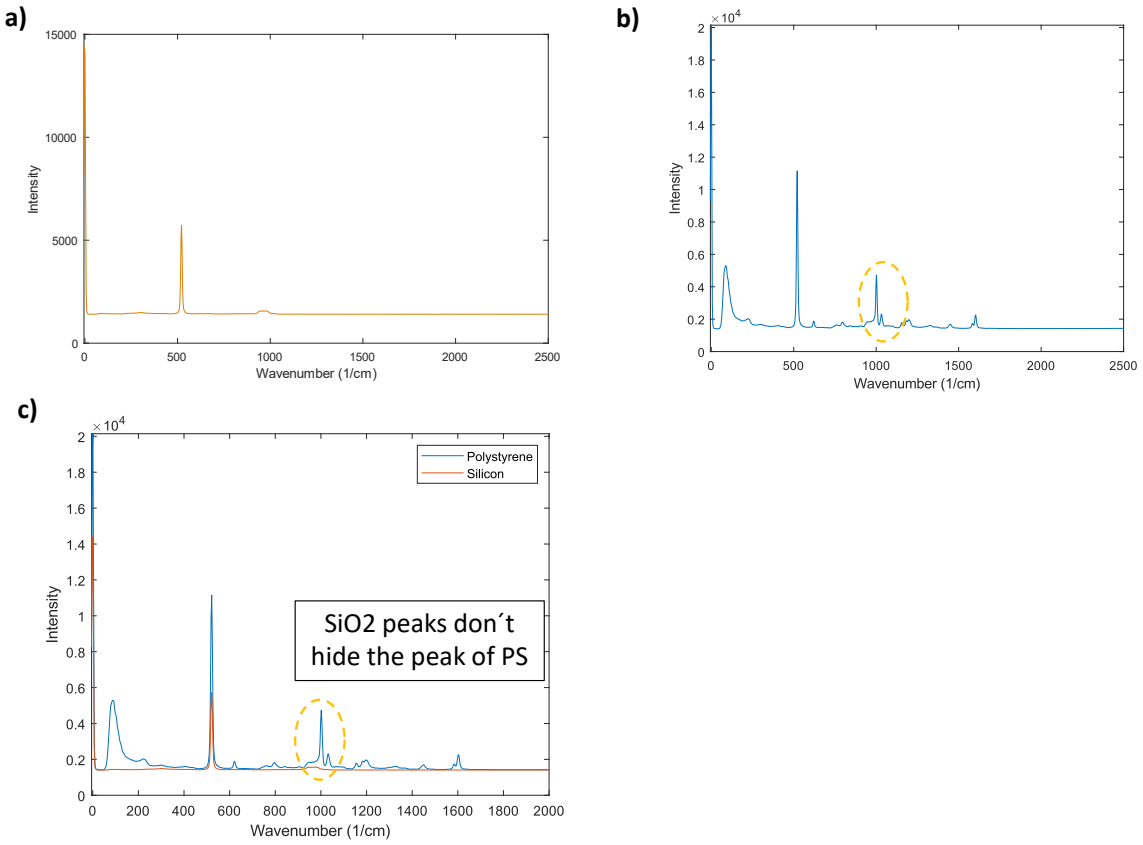

Figure 26.. b) Pure silicon substrate Raman spectra measured. c) Polystyrene Raman spectra measured. d) C-Si and PS Raman spectrums together.

Thus, while using the set-up the expected wavelength for the characterized peak can be calculated using equation (2) and showed below, where the electromagnetic incident beam is an IR laser at λ = 1310 nm. This is calculated because with the optical signal analyser it can not be measured Raman shift, the OSA only can measure power at each wavelength. For that, to measure the PS presence in the sample, we are going to measure the energy shift on the expected wavelength showed below.

$$\lambda_{detected}(nm) = \frac{1}{\frac{1}{1310\ \mathrm{nm}} - \frac{1000}{10^7}} = 1.5075 \times 10^3\ nm$$

3.3.2. Silicon Raman peak measurement and estimation

As it showed in Figure 26 a), the Raman shift is placed in 521 cm^{-1}. As in the previous section, using equation (2) it can be calculated the wavelength of the anti-stokes Raman radiation of the silicon while exciting with λ = 1310 nm. As it has mentioned before, the OSA can only measure power in each wavelength, so to make sure that the WERS experimental set-up is working correctly, and we can measure Raman signal with it, it must be calculated the expected wavelength which is going to have a shift due to the silicon Raman signal.

$$\lambda_{detected}(nm) = \frac{1}{\frac{1}{1310\ \mathrm{nm}} - \frac{521}{10^7}} = 1.4059 \times 10^3\ nm$$

3.3.3. Input fibre assembly and coupling process.

3.3.3.1. Previous work before the input fibre installation.

To be aware that every component of the set-up is operating correctly, there are some previous steps regarding the WERS experimental set-up installation. First, all the fibres, connectors, and the tip of the OF lensed were cleaned. Then, checked the losses of every component to confirm that every element is currently working correctly, the results of each component are collected in Table 3**.** It must be mentioned that the sum of the losses of each part of the set-up it will not be the total losses, because the losses of the interface between each optical element are not considered yet.

Losses measured (dBm)	
Laser	-0.1 dBm
Polarizer	-0.4 dBm
OF lensed (input)	-0.2 dBm
Sample	- 0.2dBm/cm (checked in other set-up)
OF lensed (output)	-0.3 dBm
OSA	-0.1 dBm

Table 3. Losses measured of each element of the WERS set-up.

The sample that it is used in this part, has a simple design. It has 10 parallel waveguides that cross the sample transversally. This sample it is used first for the mounting part, because it must be sure that the sample is working properly, and this sample allows the coupling process easier than samples with gold nanostructures. The substrate of the sample is made with Si_3N_4. Figure 27 shows a microscope image of the sample.

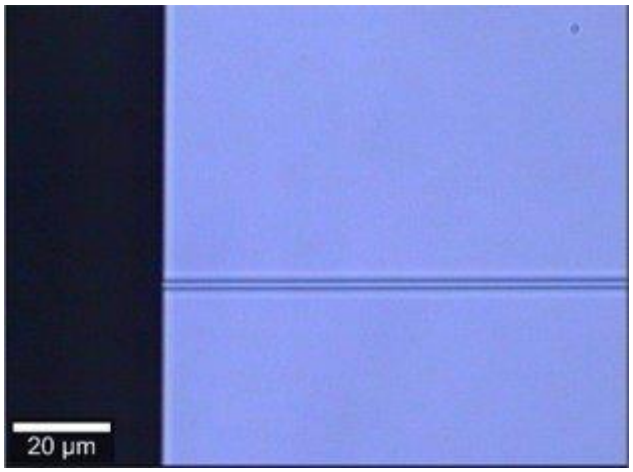

Figure 27. Microscope image of the slit waveguide used to assembly the WERS set-up

3.3.3.2. Input fibre assembly

For the first part, one 3D stage was assembled for the coupling process of the input optical fibre. Next to this stage was positioned a 2D stage, this stage is where the sample is positioned with doble-side tape and allows the movement in directions “x” and “z”, as it is shown in Figure 28. Therefore, on the other side of the sample, was assembled a 4D stage, which allows movement in the 3 axis and rotation around “z” axis. On this stage was positioned a collimator (objective), the collimator captures the output beam of the sample and transmitted it parallel to the ground line, directly to an infrared camera. The infrared camera was positioned in a 4D stage, too.

For the coupling process, the set-up has two points of view. The first one is a microscope above the sample (O1), the second one is a USB microscope (O2) on the perpendicular direction of the sample, as it shown in Figure 28. With these two points of view, the set-up has vision of the fibres and sample in the 3 axes, making able the coupling process.

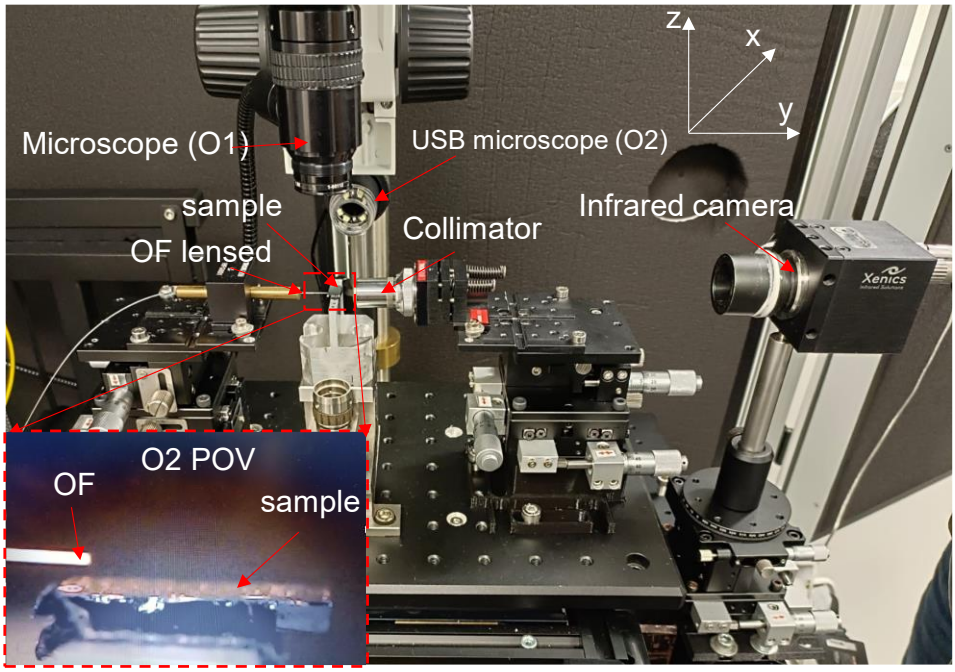

Figure 28. Experimental set-up to measure wave-guided Raman radiation.

The first approach of the set-up features with a collimator, in other words, with a free-space part. But this is necessary to couple the input fibre to the sample, in a process that would be impossible without a free space part, because the wavelength chosen is in the IR band.

It is necessary to mention that the input OF is a fibre lensed, that means, it has a tip ending, as it shown in Figure 8 a). The tip ending makes possible to couple the light in transmission configuration without any nanostructure such as gratings or broadenings.

3.3.3.3. Coupling process

The coupling process of the input fibre is divided into 2 parts. The first part consists in the alignment of the fibre, collimator, and camera, as it shown in Figure 29 a). The second part consists in the alignment of the fibre and the waveguide, as it shown in Figure 29 b).

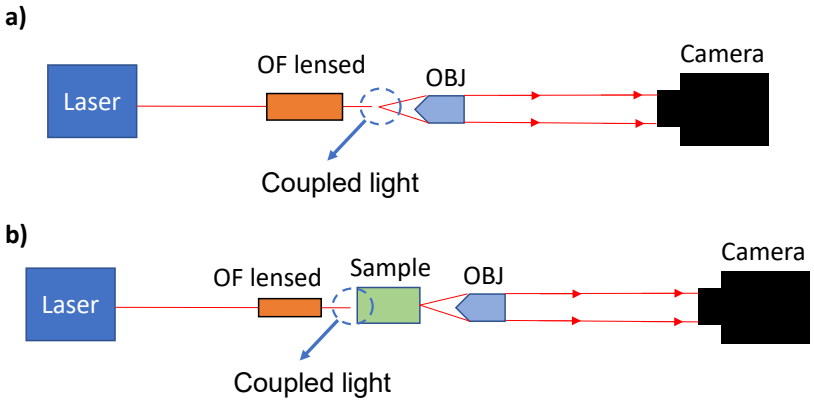

Figure 29. a) Coupling process fibre, collimator, and camera conceptual map. b) Coupling process fibre and waveguide conceptual map.

1) In order to couple fibre-collimator-camera, first check the beam with an infrared card detector. So, for a first approach it can be done the alignment with the infrared card. Then, the fibre must be approached to the collimator while adjusting the collimator height until is reached

the focal distance, as it shown in Figure 30 a) , the pattern displayed in the infrared camera will be like Figure 30 a).

2) Secondly, to couple fibre-waveguide, is necessary to approach the fibre tip above and near to the sample, like Figure 30 b). Then, align the fibre with the waveguide, and will be displayed the pattern showed in Figure 30 c) on the infrared camera software.

3) At this point, displace the fibre in "-y", to stop being above the sample. Then, guiding via O1 scroll down very slowly the input OF in "-z", the diffraction pattern will be disappearing, until the infrared camera displays the spot, which will look like Figure 30 d). The spot means that the fibre is coupling light in one single mode correctly.

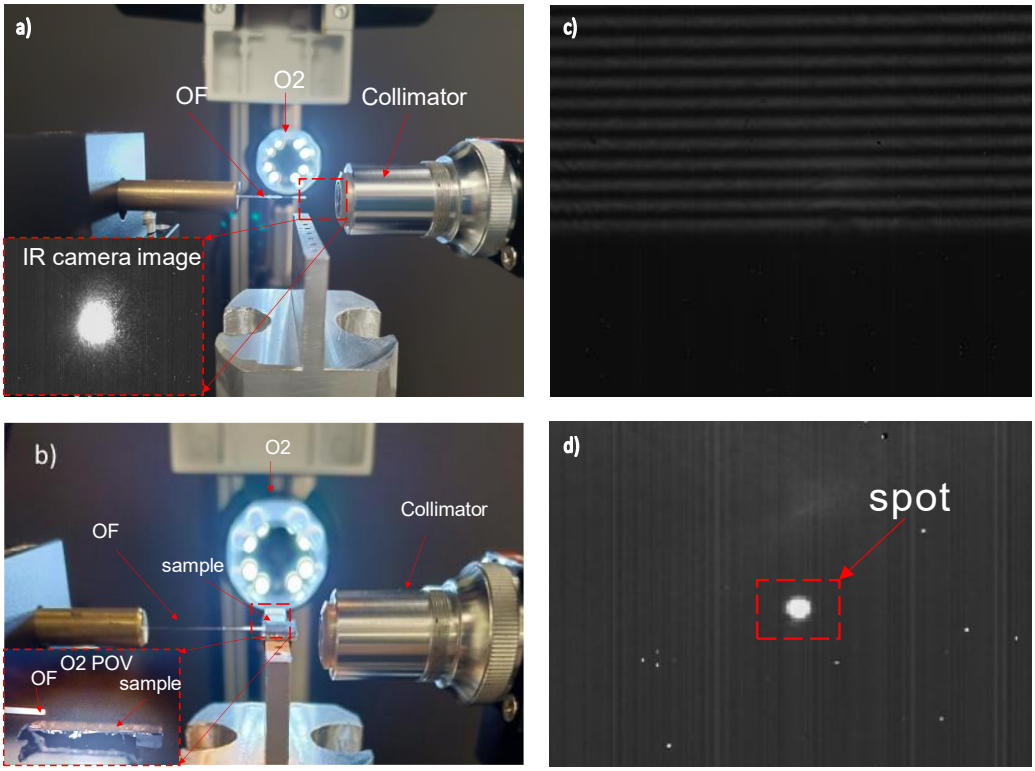

Figure 30. a) Fibre coupled to the collimator. b) Process of coupling the fibre to the waveguide. c) Diffraction pattern displayed on the infrared camera software when the fibre is above the sample. d) Spot pattern displayed on the infrared camera software when the fibre is coupled to the waveguide.

3.3.3.4 Power beam optimization

In order to check the power beam coupled to the waveguide, it was necessary to add to the set-up some new components. Firstly, a beam splitter (BS) to split the beam was added, one beam directly to the camera and the other directly to the power meter that was added in this step, too. The actualization of the new set-up is illustrated in Figure 31 a) and b).

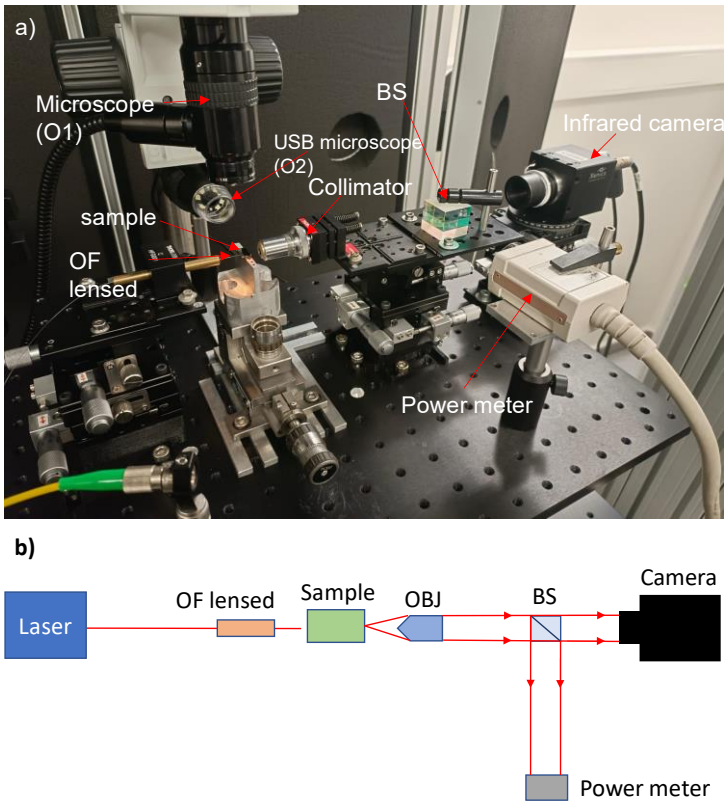

Figure 31. a) Image taken of the real set-up with a beam splitter and a power meter assembled. b) Set-up scheme.

The power reported with this configuration was around -60 dBm. So, using this configuration did not allow us to do check tasks because of the high losses measured. Therefore, the set-up for checking the power coupled was changed.

The beam splitter was removed, and the power was directly checked from the beam. As the power meter cap can be easily placed in anywhere of the beam pathway, it was decided to choose 3 different places to measure the losses, because it was noticed that the beam was not collimated when it was checked with the infrared card. First, the power right next to the output of the collimator (P_1) was checked. Then, the power was checked in the middle of the collimator and the infrared camera (P_2) and in the same place of the camera (P_3), because the camera can be changed for the power meter, as it illustrated in Figure 32 a). The results reported are collected in Table 4.

Losses measured (dBm)	
P_1	-8 dBm
P_2	-6 dBm
P_3	- 5 dBm

Table 4. Losses measured in the three places specificized of the set-up while coupling fibre-objective.

The results show what expected, in the camera, the collimator focus the beam and less losses are reported. Furthermore, for this typical set-up -5 dBm in this part is a normal value of losses.

To check the losses while coupling the fibre and the waveguide it was followed the same methodology and changed the infrared camera for the power meter to check the power. Figure 32 b) illustrates the set-up configuration for this free space losses measurements and -15 dBm of losses were reported. Considering the interfaces between each optical component and the length of the sample (L =3 cm) we can assume that -15 dBm is a reasonable lost for this part.

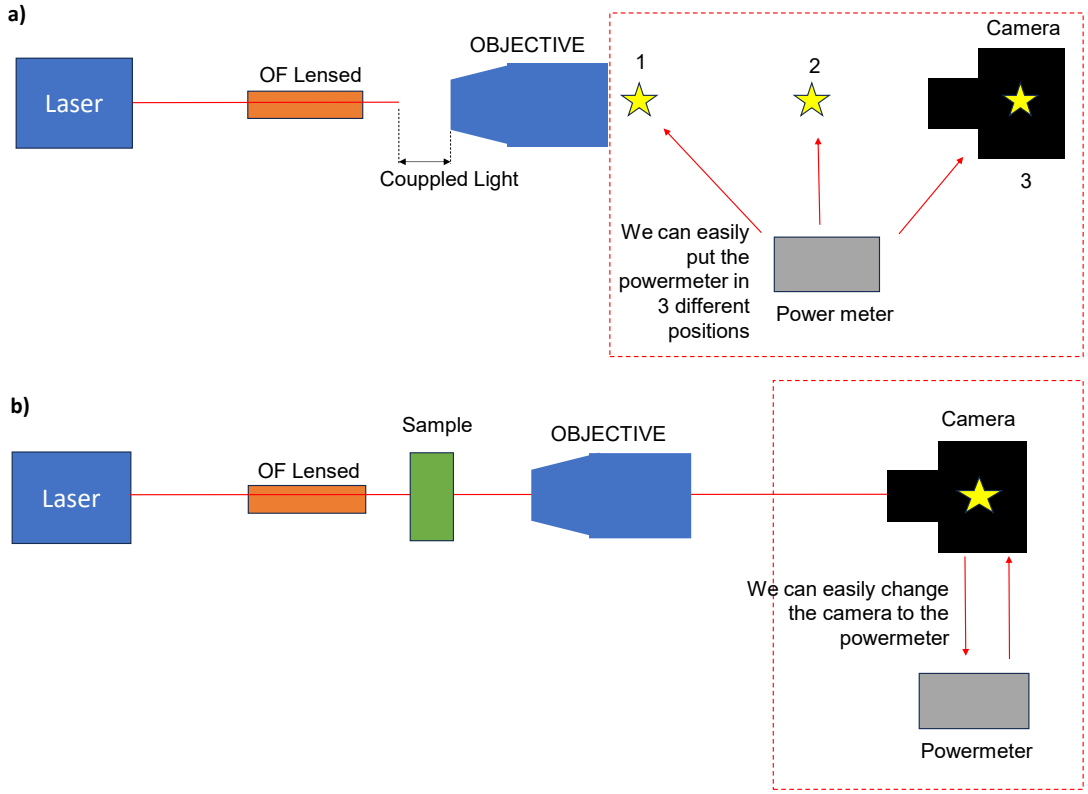

Figure 32. a) Set-up configuration for free space power measurements for the OF lensed coupled to the objective. b) Set-up configuration for free-space power measurements for OF lensed coupled to the waveguide.

3.3.4. Output fibre installation and coupling process.

3.3.4.1. Output fibre installation

Once is demonstrated that the input part of the set-up has a correct power and minimal losses, the next step is to assembly the output fibre and explain the coupling process. Thus, it was installed an optical fibre holder in the 4D stage which is the collimator. So, as it has 3 degrees of freedom (DOF) and rotation around "z" axis, the system allows to couple the input fibre and then rotate 90º degrees to couple the output fibre, the mechanism is illustrated in Figure 33. The set-up was designed like this, because the space is limited on the bench work, so it could not be done with two 3D stages and a system of rails as it typically done in this type of optical set-ups. Thus, it was discussed the most efficient way to assembly was this mounting. The output fibre is directly connected to the OSA with an FC connector.

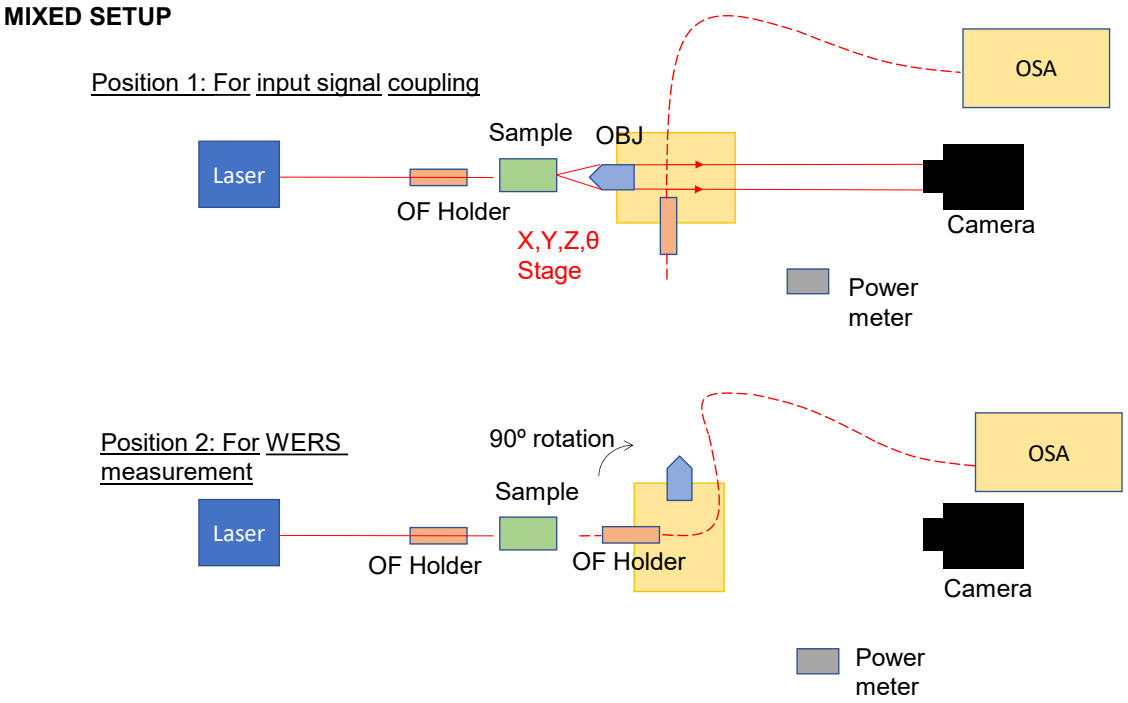

Figure 33. Scheme for the set-up with the rotation 3D stage to change for input signal coupling (position 1) and for WERS fully guided measurements (position 2).

As well as it was done in the previous section, it was necessary to choose a type of fibre. In this case, it is compared the power of the beam of two fibres coupled by measuring the losses. First, a OF lensed coupled with another OF lensed was used. Then, it was measured the losses with a OF lensed coupled with a OF cleaved. The results obtained are in Table 5 and the process illustrated in Figure 34.

Fibres coupled	**Losses measured (dB)**
Lensed to lensed	- 4 dB
Lensed to cleaved	-12 dB

Table 5. Power losses measured in a coupled fibre lensed to fibre lensed and to a cleaved fibre.

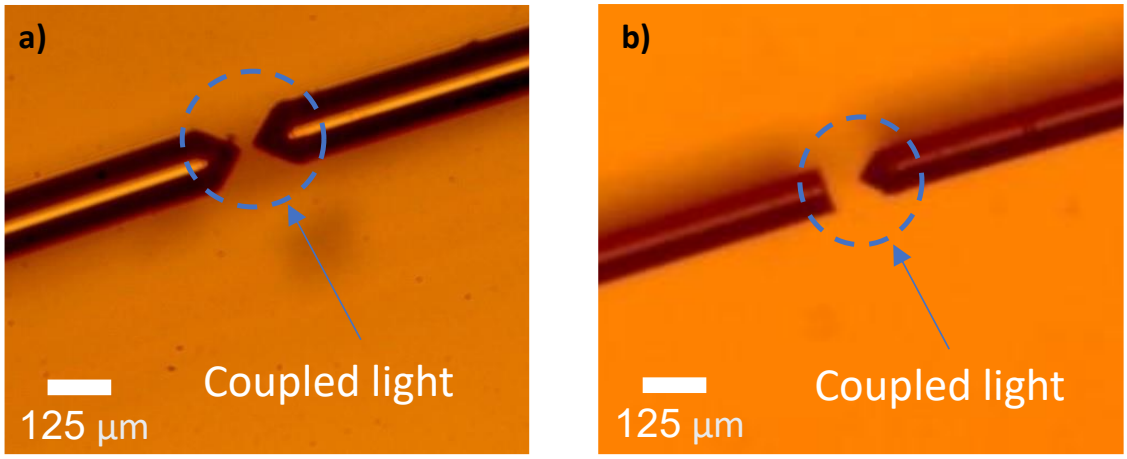

Figure 34. a) Fibre lensed coupled to a fibre lensed. b) Fibre lensed coupled to a fibre cleaved.

3.3.4.2. Output fibre coupling process

The process of coupling the output fibre is significantly different from coupling the input fibre, because it can't be used any free space method to guide the coupling process, because on the other side of the sample is already coupled the input fibre. Thus, in the current section it is explained the methodology utilized to check the correct assembly of the set-up and the coupling process.

1) First, as the set-up has a rotatory stage, it must be checked the angle of the fibre. If it is not checked, it would be several losses. For that, the output fibre was placed above the sample and aligned with any waveguide, while observing the microscope (O1) image to proof that the waveguide and the fibre core are parallel lines.

The next step it was only necessary to do it the first time, to be sure that the set-up was able to couple the light.

2) In the next step was checked that our fully integrated system was able to couple light by coupling red light (λ = 633 nm). Figure 35 illustrates the real set-up while both fibres coupled. Then, changed to the IR laser (λ = 1310 nm) and adjusted the coupling.

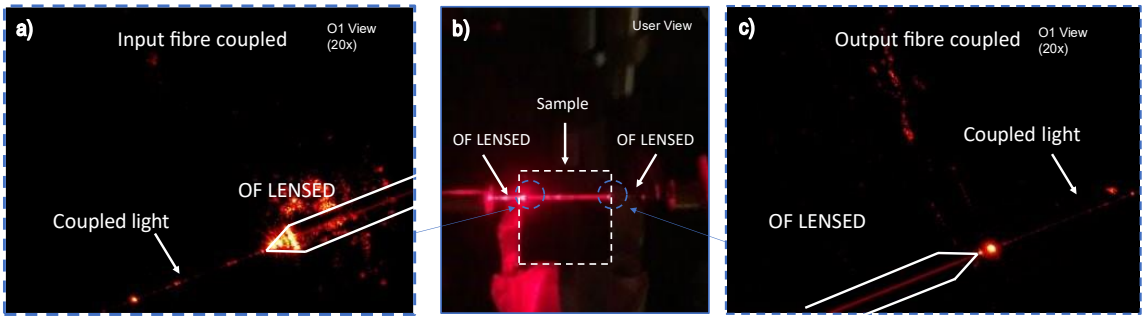

Figure 35. a) Image taken of the set-up while coupling red light with camera. b) Image taken of the input fibre coupled to the sample with microscope (x20). c) Image taken of the of the output fibre coupled to the sample with microscope (x20)

Thus, for all the following coupling processes it wasn't necessary to do the coupling process with red light, but it can be useful for guiding the alignment process.

3) Finally, place the output fibre next to the sample and move on "-z" until the power meter starts measuring power. Then, adjust the fibre position to minimize the losses.

It must be mentioned that the coupled process with an IR laser would be done like step 2, if it was used an infrared microscope above the sample. Because the free space optical elements would not be necessary and just by looking at the image of this ideal camera, the IR beam can be coupled.

3.3.5. Optical elements for measuring the signal.

Final part, consist of the first approach of optical elements used to measure guided Raman signal. First, it is explained the characterization of a Booster Optical Amplifier (BOA) used to enhance the input power. Then, the final measurements with an optical signal analyser are reported.

3.2.5.1. Booster Optical Amplifiers

In this section it is explained the characterization of a booster optical amplifier used to enhance the Raman signal.

First, it was tried to use the BOA to enhance the input beam, because enhancing the input beam will reduce the power lost in the sample. But, using the BOA directly before the laser could produce backscattering and subsequently this could cause damage in the laser. To avoid that, an isolator was placed between the laser and the BOA. Figure 36 illustrates the mentioned set-up.

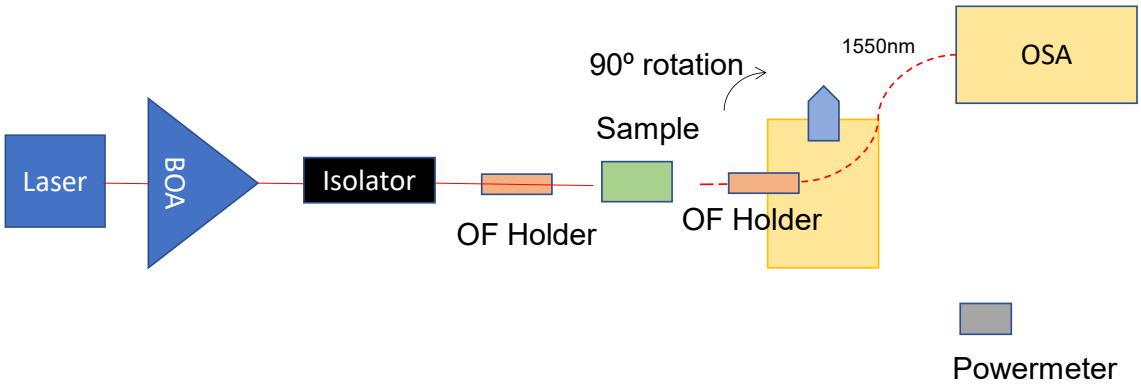

Figure 36. Set-up configuration with a BOA and an isolator to enhance the input power of the beam.

Table 6 summarizes the performance of the BOA. It has to be mentioned that 550 mA is the maximum to amplify, then the amplifier is saturated. That means that it can be amplified anymore. On the other hand, non-linear regime starts when the optical output reach 11 dBm. Thus, it does not make sense to amplify the laser beam, it can be reached 13 dBm because using only the laser. So, the difference between 13 dBm and 20 dBm of input power it is not high enough to be considered as an advantage and place the isolator and the BOA in the first part of the set-up.

Laser (dBm)	BOA (mA)	Power meter (dBm)
-15	550	10.85
-13	550	11.55
-10	550	12.74
-7	550	14.23
-5	550	15.3
-1	550	17.13
0	400	17
0	550	17.8 (saturation)
2	550	18.9
5	550	19.9
7	550	20
9	550	20.3
13	550	20.5
OFF	550	9.99
0	OFF	-14.3
OFF	OFF	LOW

Table 6. Laser power measured in decibelios-miliwatio (dBm), BOA intensity of amplification measured in milliamperes (mA) and power measured before the isolator and amplifier (dBm)

The final losses measured were -30 dBm with this configuration. These losses were too much for measuring guided Raman signal. Therefore, some changes were evaluated, finally measuring guided Raman signal. These changes are not presented in this chapter because it wasn't done, so it is discussed in the next section.

On the other hand, creating images of the sample creates a further understanding of the photonic phenomenon occurring during the experiments. As a new dimension is added to the measured signals, a further knowledge is added to the measurements. Indeed, adding the ability to create light images of the sample improves the understanding of the results obtained. So, as it was described before in the introduction, another line of future development could be assembling a SNOM cap to measure near field light signal of the sample. By the way, the SNOM

cap it was assembled to the set-up, but no experiments were made to measure the performance of the cantilever. Figure 37 shows the head assembled to the current set-up.

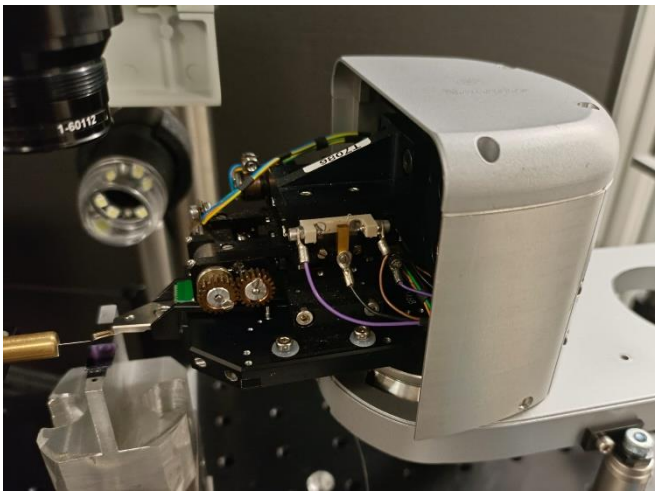

Figure 37. NSOM head assembled to the set-up for near-field light images.

3.4. FINAL CONSIDERATIONS

WERS substrates it's a potential tool for biosensing applications. But a widely work has to be done before a real product can be released. For that, in this section are presented some filters, and other laser wavelengths estimations and methodologies that can be used to improve the WERS experimental set-up.

To begin with, WERS set-up can be improved in two different ways. First path to follow is improving the signal received to the OSA by filtering it. In order to do this step fully integrated several options were studied. The possible three options commercially available with the range of at least the polystyrene anti-stokes Raman radiation shift while exciting with 1310 nm are showed in Figure 38. Furthermore, Figure 38 a) is the best option, because it has the littlest span of them three. This is a relevant factor while purchasing a filter because noise it is also amplified while using it. So, a filter with a wide range of working will enhance a lot the noise and occult the Raman signal. But it must be considered that filter b) it's also a good option. Although it has a wide span of 100 nm, the centre wavelength can be chosen at any between 300 nm and 2400 nm. This allow to measure the silicon Raman peak, which is also an advantage while assembling the set-up, because polystyrene droplets sometime will be evaporated. The last option is the wideband tunable fibre optical filter, which is the worst option, because its range only reach the polystyrene Raman peak and its span is very wide.

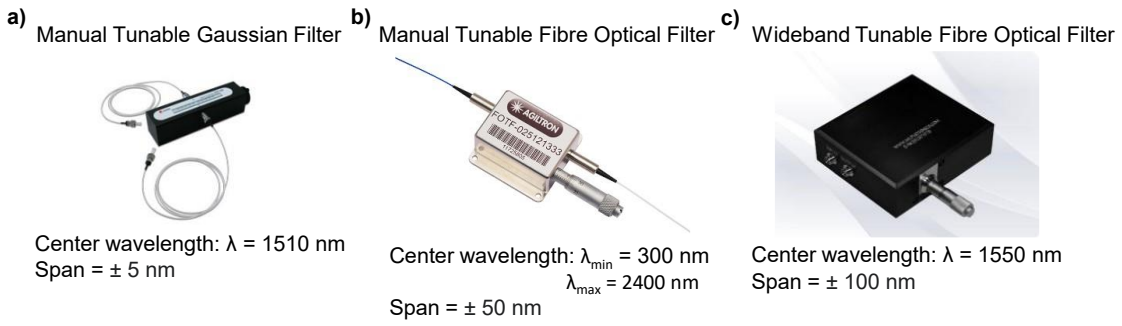

Figure 38. a) Manual tunable gaussian filter. b) Manual tunable fibre optical filter. c) Wideband tunable fibre optical filter.

Along the same line after filtering, an amplifier can be used to first enhance the silicon peak. Then when the set-up is measuring the silicon Raman signal, enhance the polystyrene Raman radiation. But the problem here is that there are not commercially available Erbium Dopped Optical Fibre (EDFA) amplifiers working in the spectra of silicon and polystyrene Raman anti-stokes wavelength while exciting with 1310 nm. For that, it can be considered exciting in a certain wavelength that allows to measure either the Raman anti-stokes silicon or polystyrene peak at 1550 nm, a certain wavelength with multiple amplifiers and filters already commercially available due to the several applications in the field of telecommunications. Therefore, the estimation can be calculated with equation (2).

Silicon: $$\lambda_{incident}(nm) = \frac{1}{\frac{1}{1550\ \text{nm}} + \frac{521}{10^7}} = 1434\ nm$$

Polystyrene: $$\lambda_{incident}(nm) = \frac{1}{\frac{1}{1550\ \text{nm}} + \frac{1000}{10^7}} = 1341.99\ nm$$

Thus, while exciting with 1310 nm, in the OSA it will be expected to measure a peak at these wavelengths.

To sum up, losses, either caused by propagation along imperfectly-etched waveguides or by coupling from and to the output fibre, are a very important roadblock towards efficient WERS. Therefore, additional work is needed to improve the photonic chip. But remarkably, one the waveguides are done, the inclusion of plasmonic nanostructures as the NPoM addressed in this work, should pave the wave towards highly-compact WERS avoiding very large dielectric waveguides

CHAPTER 4. CONCLUSION

4.1. CONCLUSION

To summarize, several objectives were completed. First, surface functionalization with BPT were made on samples with nitride silicon waveguides integrated with a gold resonant nanostructure. Second, nanoparticle transfer was made onto the gold surface to measure Raman radiation. Finally, the assembly of a setup for WERS measurements at 1310 nm were doe.

To begin with, sample preparation of photonics integrated chips (PICs) was done. First, samples were functionalized with BPT. Then, gold spherical nanoparticles of two sizes 60 nm and 150 nm were transferred onto the gold Raman resonance nanostructures. This creates the NPoM configuration that enhances the electric field in the nanocavity between the NP and the gold surface where the molecular monolayer is assembled and allows to measure Raman signal. Several methodologies were followed to achieve this objective. First, nanoparticles were transferred by drop casting, reaching to successfully transfer one nanoparticle into the gap of a gold nanoantennae of sample c) and measure guided Raman spectra of BPT identifying 1100 cm^{-1}, 1300 cm^{-1} and 1600 cm^{-1} characteristics peaks. Two modes of polarization were used: TM and TE and confirmed that TM creates a higher intensity of the Raman radiation because of the higher interaction between the electric field and the molecule. Furthermore, the Raman spectra was measured using the red laser beam, because with λ = 532 nm a highly fluorescence noise was measured and the BPT peaks were hidden. Also, during the process drop casting methodology was catalogued as a poor to technique to do this process, due to its low accuracy on sample a).

Therefore, accurate transfer methodology to transfer single nanoparticles onto gold nanostructures was used. Both methodologies used, were made by soft-lithography using a PDMS mask. First methodology used PDMS to sweep the nanoparticles into the slits of a sample. For sample e), nanoparticles were identified using BF and DF microscopy. DF microscopy allowed to identify nanoparticles easier than using BF microscopy in samples with a high number of gold Raman active nanostructures. Also, SEM microscopy and Raman imaging of the sample was used to characterize it. Free space Raman spectrums were used to confirm the presence of the BPT in the sample. The second methodology used the PDMS to stamp the NPs into the gap of a gold nanoantennae with an 80 nm gap of the sample a). In only one attempt, the accuracy of the method was increased than using drop casting. The BPT guided Raman spectrum was measured by using the conventional Raman spectrometer. Thus, leads the current work to reach the second main objective: creating a specific set-up for guided Raman for characterizing the samples.

For the assembly of the WERS set-up, several steps were presented. First, silicon and polystyrene Raman shift was measured. Then, anti-stokes Raman shift was determined using equation (2) presented in the review of Raman spectroscopy. Subsequently, WERS set-up assembly was

explained, cleaning and checking the losses of each optical component was the first step. Next, input fibre parts were assembled, coupled in free space, and checked the power losses. Then, a rotatory stage was assembled to coupling the output fibre and the importance to have an infrared camera above the sample is underlined. Because, with an infrared camera taking images of the lithography the coupling process of an IR laser will be the same as a visible laser. Finally, an amplifier is characterized, the current state of the set-up with the NSOM head is showed and the final considerations are presented. For this last part, some objectives were not accomplished. These objectives are to take guided Raman measurements of the 521 cm^{-1} peak and 1000 cm^{-1} polystyrene's peaks. Furthermore, the prepared samples could not be characterized with the WERS set-up. We think that the coupling losses (from the fibre to the chip and vice versa) as well as the propagation losses could explain the absence of the expected Raman peak in our final measurements.

Finally, as it has mentioned before, this project is part of a final system that will be developed by one of my supervisors Dra. Elena Pinilla Cienfuegos, included in a research article presented in the *Fuerzas y Túnel 2023* congress (https://aseva.es/conferences/fuerzas-y-tunel-2023/).

4.2. FUTURE WORK AND IMPACT

This section underlines the impact that the work will have on the NTC facilities and in other futures works. Two considerable factors can be potentially used for other doctoral works or degree final thesis. On the one hand, samples prepared can be used to create a specific biosensor for a specific analyte. As it has been demonstrated the hybrid waveguide-surface enhancement of the nanoparticle deposited in the gap of several nanoantennaes of different samples, the next step is to create a specific bonding for an analyte with the sample. For that, a bioreceptor of a relevant analyte of health concerns such as cancer's biomarkers, DNA fragments of antibodies resistant bacteria, SARS-CoV-2 spike protein, drug biomarkers or VIH biomarkers can be chosen. Then, a bioreceptor for label-free biosensors must be selected. Nowadays, nanotechnology and biotechnology bring the opportunities to create a specific bioreceptor with a higher specificity. For instance, aptamers could be used for DNA or protein recognition with specificity and the advantage of having thermal stability instead of using monoclonal antibodies [34, 35, 36]. Next, step would be to make the ANOVA test for the response of the sensor between the analyte Raman peak intensity and a buffer base line. Then, creating the calibration curve of the sensor, working range, limit of detection and working range (WR).

On the other hand, the future functional biosensor or other Raman based biosensors can be characterized with the specific assembled set-up. When the set-up is optimized for taking measurements, Raman active chips can be characterized easier than using the conventional Raman spectrometer. As a follow-up of this work, the prepared samples can be characterized with the WERS set-up when is ready to take guided Raman measurements. Furthermore, the NSOM cap will allow to create light imaging of Raman samples, that would allow to create a better way to measure the signal than using an OF lensed and transmission measurements. With the rise of artificial intelligences (AI) images can be an excellent tool for creating a future device for investigation laboratories. For a future line of developing a portable device, several attempts in the literature have been made. Article [14] report an interesting way to package the sensor.

As the main problem of a fully integrated sensor is package the fibres coupled with the waveguides of the sample. In the same article it is created a package with microfluidic channels with epoxy that join fibres and sample coupled.

The ultimate goal would be the realization of samples with NPoM structures, which have demonstrated an ultimate light localization leading to the most efficient Raman signal excitation and collection, from all SERS structures developed so far, integrated with silicon nitride waveguides for excitation and collection, and that can be measured in the 1310 nm window. This approach, which is strategic for the NTC institute, has several advantages over existing approaches, namely:

- It includes the NPoM cavity to enhance the Raman scattering efficiency as a result of the localization of the light in nm-scale regions.

- It includes waveguides for effectively injection of the pump and collection of the Raman signal.

- The realization in silicon technology means low-cost massively produced chips.

- The use of waveguides instead of free-space excitation and collection also leads to the possibility of massive multiplexing using multiple waveguides, which would allow for detection of multiple substances on a single chip.

- The use of 1310 nm wavelength benefits from the advanced optical equipment (lasers, photodetectors, filters, amplifiers) available at that wavelength and developed for optical communications in the 2nd telecom window.

UNIVERSITAT POLITÈCNICA DE VALÈNCIA

ESCUELA TÉCNICA SUPERIOR INGENIEROS INDUSTRIALES VALENCIA

BUDGET

Design of a waveguide-nanoparticle enhanced Raman scattering system for advanced on-chip spectroscopy

CHAPTER 5. BUDGET

5.1. INTRODUCTION

This document provides a detailed description of the economic resources used to develop this project, considering the labour, machinery and materials used in each of the phases.

The workforce consists of a biomedical engineer student and two co-tutors of the thesis, who oversee the student's workflow supervision. To simply the budget calculation, only the contribution of one tutor's labour will be assumed. Furthermore, the cost of the student labour is calculated using equation (11).

$$Worker\ cost = Gross\ salary + Social\ security\ cost \quad (7)$$

The Social security cost (SSC) is determined by using percentages of the employee's gross salary. Considering 23.6% as the contribution for common contingencies, 5.5% for the unemployment contribution for permanent contracts, 1% for the contribution for accidents at work and occupational diseases for office workers, 0.6% the quotation for vocational training and 0.2% the contribution to the *Fondo de Garantía Salarial* (FOGASA). The cost is calculated in equation (12).

$$Social\ security\ cost = Gross\ salary\ x\ (0.236 + 0.055 + 0.01 + 0.006 + 0.002) \quad (8)$$

Considering the holiday period and annual bonus, it is estimated that the annual salary of an engineering student is 1100 euros, while the salary of the tutor as a university professor is around 3500 euros. The annual SSC for the biomedical engineering student (ST) is calculated in equation (13) and for the professor tutor (PT) in equation (14).

$$Annual\ SSC\ ST = 4.078{,}8\ \frac{€}{year} \quad (9)$$

$$Annual\ SSC\ PT = 12.978 \frac{€}{year} \quad (10)$$

And the annual cost for the student and the professor respectively:

$$Annual\ ST\ cost = 1100 \frac{€}{month} \times 12\ \times 4078.8 \frac{€}{year} = 17.278{,}8\ \frac{€}{year} \quad (11)$$

$$Annual\ PT\ cost = 3500 \frac{€}{month} \times 12\ \times 12978 \frac{€}{year} = 54.978\ \frac{€}{year} \quad (12)$$

Discounting free days and holidays, the working days remaining in a year are 224, for 8 hours working each day, the hourly cost of each person remains:

$$Hourly\ ST\ cost = \frac{17.278{,}8\ \frac{€}{year}}{224\frac{days}{year} \times 8\frac{hours}{day}} = 9.64\ \frac{€}{hour} \quad (13)$$

$$Hourly\ PT\ cost = \frac{54.978\ \frac{€}{year}}{224\frac{days}{year} \times 8\frac{hours}{day}} = 30.68\ \frac{€}{hour} \quad (14)$$

Being 9.64 euros at hour for the student and 30.68 for the tutor.

For the machinery amortization costs provided by the Nanophotonics Technology Centre (NTC), it is considered 45 €/hour per equipment. Finally, from the partial budgets, the total budget for material execution is obtained by adding 13 % overheads and 6% of industrials profit, and 21% for VAT in order to obtain the total budget.

5.2. DETAILED BUDGET

The detailed budget was obtained using the software CYPE ARQUIMEDES student version. It consists of the several tables below:

- Table 1. Labour cost table.
- Table 2. Machinery cost table.
- Table 3. Materials cost table.
- Table 4. Unit price cost table.
- Table 5. Partial budget.
- Table 6. Contractual implementation budget.

Table 1. Labour cost table

Labour Table — Page 1

Num.	Code	Labour designation	Price	Hours	Total
1	L.03	Thesis tutor distinguished reseacher	33,400	2,000 h	66,80
2	L.04	Thesis tutor cathedratic in photonics	33,400	2,000 h	66,80
3	L.PHD	Thesis tutor phd in photonics	30,680	178,000 h	5.461,04
4	L.IBE	Biomedical engineer student	9,640	230,000 h	2.217,20
				Total mano de obra:	7.811,84

Table 2. Machinery cost table

Machinery table — Page 1

Num.	Código	Machinery designation	Price	Quantity	Total
1	EQ.LIT	Raith 150 (lithography)	500,000	1,000 u	500,00
2	EQ.ET	Etching: RIECIP	90,000	2,000 u	180,00

3	EQ.BM	Brewer Model (Aged and Developed)	50,000	1,000	u	50,00
4	EQ.PVA	Tepla PVA	50,000	3,000	u	150,00
5	EQ.R	Coater EVG 101	50,000	1,000	u	50,00
6	EQ.BENCH	Optical bench	45,000	20,000	h	900,00
7	EQ.3D	3d printer	45,000	4,000	h	180,00
8	EQ.ISO	Isolator (C00SS0021)	45,000	20,000	h	900,00
9	EQ.LASER	Tunable semiconductor laser TSL-570 (1260nm - 1360 nm) SANTEC	45,000	20,000	u	900,00
10	EQ.IR	Infrared camera XENICS	45,000	20,000	h	900,00
11	EQ.DF	Microscopio de campo oscuro	45,000	16,000	h	720,00
12	EQ.BOA	Booster optical amplifier THORLABS S9FC1132P	45,000	20,000	h	900,00
13	EQ.OSA	Optical signal analyzer HP HEWLLET PACKARD 26142A	45,000	20,000	h	900,00
14	EQ.MCAMERA	Camera adapted for use with microscope	45,000	20,000	h	900,00
15	EQ.NPtransfer	NP set-up transfer	45,000	1,000	h	45,00
16	EQ.US	Ultrasonic cleaner	45,000	0,083	h	3,74
17	EQ.Sim	CST STUDIO SUITE (simulation)	45,000	3,000	h	135,00
18	EQ.SOURCE	Light source SCHOTT	45,000	20,000	h	900,00
19	EQ.SEM	Scanning electron microscope (SEM)	45,000	5,000	h	225,00
20	EQ.RA	Espectrómetro alpha300 (Raman-AFM) (WITEC)	45,000	68,000	h	3.060,00
21	EQ.RAs	Software Project 4.0 (Witec)	45,000	68,000	h	3.060,00
22	EQ.VFL	Visual Fault Locator	45,000	20,000	h	900,00
23	EQ.LO	Licencia Libre Office	0,001	40,000	h	0,04
24	EQ.PCp	Portátil	0,001	43,000	u	0,04
25	EQ.LW10	Licencia Windows 10	0,001	50,000	h	0,05
26	EQ.LO365	Licencia de Office365	0,001	50,000	h	0,05
27	EQ.WI	Windows 10 License (UPV)	0,001	1,000	u	0,00

Total machinery: 16.458,92

Table 3. Materials cost table

Materials table

Num.	Code	Material designation	Price	Quantity	Total
1	MAT.SNOM	NSOM probe 200 nm Cr-Au	1.598,500	1,000 u	1.598,50
2	MAT.P	Polarizer	323,370	1,000 u	323,37
3	MAT.mPIP	Micropipette 10-100 ?L	310,510	3,000 u	931,53
4	MAT.O	Wafer SOI	250,000	1,000 u	250,00
5	MAT.COLL	Collimator THORLABS	214,750	1,000 u	214,75
6	MAT.NP150	150 nm diameter gold spherical nanoparticles	195,000	2,000 L	390,00
7	MAT.PDMS	PDMS	170,000	1,000 m3	170,00
8	MAT.MP2	Machlifg LT60-LM XYZR 4-Axis LInear stage, rotation and goniometer	159,000	2,000 u	318,00
9	MAT.NP60	60 nm diameter gold spherical nanoparticles	155,000	2,000 L	310,00
10	MAT.MICRO	Optical microscope	120,000	1,000 u	120,00
11	MAT.MP	Machlift 60x60mm XYZ 3-Axis Linear Stage	119,000	2,000 u	238,00
12	MAT.USB	USB Microscope	79,000	2,000 u	158,00
13	MAT.AFM	AFM tips	50,000	2,000 u	100,00
14	MAT.PM	Power meter AQ2140 OPTIMAL MULTIMETER	45,000	20,000 h	900,00
15	MAT.PMsensor	ANDO AQ2743 SENSOR	45,000	20,000 h	900,00
16	MAT.BPT	BPT (Biphenyl-4-thiol)	44,500	1,000 u	44,50
17	MAT.ET	Ethanol	28,800	1,000 L	28,80
18	MAT.B	Laboratory coat	15,000	1,000 u	15,00
19	MAT.STC	Carbon conductive tape, double coated	14,000	2,000 u	28,00
20	MAT.TIP	Micropipette tips	11,500	7,000 u	80,50
21	MAT.H2SO4	Sulfuric acid	6,600	1,000 L	6,60

22	MAT.OF	Optical fibre lensed	6,450	2,000 u	12,90
23	MAT.G	Nitrile gloves	5,820	1,000 u	5,82
24	MAT.CLAMP	Laboratory clamps	5,100	4,000 u	20,40
25	MAT.H2O2	Hydrogen peroxide	2,500	1,000 L	2,50
26	MAT.CAMP	Exhaust hood	2,060	6,000 h	12,36
27	MAT.GLASS	Glass vial	1,640	2,000 u	3,28
28	MAT.N2	N2 stream	1,400	33,000 m3	46,20
29	MAT.H2O	Ultrapure water	1,250	3,000 L	3,75
30	MAT.OF_f	Fibre optic	0,600	2,000 m	1,20
				Total materials:	7.233,96

Table 4. Unit price cost table

Unitary price cost table			
Nº	Designation	Import	
		Number (Euros)	Word (Euros)
	1 Project definition		
1.1	u Initial meeting with thesis' tutors	107,12	ONE HUNDRED EUROS AND TWELVE CENTS
	2 State of the art investigation		
2.1	1 State of the art	1.612,84	ONE THOUSAND SIX HUNDRED TWIELVE EUROS AND EIGHTY-FOUR CENTS
2.2	1 Theoretical-practical formation	1.402,56	ONE THOUSAND FOUR HUNDRED TWO EUROS AND FIFTY-SIX CENTS
	3 Methodology and results		
3.1	u Theoretical sample design and microfabrication	1.355,32	ONE THOUSAND THREE HUNDRED FIFTY-FIVE EUROS AND THIRTY-TWO CENTS

3.2	u BPT functionalization	690,96	SIX HUNDRED NINETY EUROS AND NINETY-SIX CENTS
3.3	u Nanoparticle transfer by drop casting	1.511,66	ONE THOUSAND IVE HUNDRED ELEVEN EUROS AND SIXTY-SIX CENTS
3.4	u Nanoparticle transfer with PDMS stamp	934,26	NINE HUNDRED THIRTY-FOUR EUROS AND TWENTY-SIX CENTS
3.5	u Sample characterization	7.795,90	SEVEN THOUSAND SEVEN HUNDRED NINETY-FIVE EUROS AND NINETY CENTS
3.6	u WERS set-up assembly	14.598,56	FOURTEEN THOUSAND FIVE HUNDRED NINET-EIGHT EUROS AND FIFTY-SIX CENTS
	4 Dissertation writing and correction		
4.1	u Dissertation writing	482,10	FOUR HUNDRED EIGHTY-TWO EUROS AND TEN CENTS
4.2	u Correction of the documents	422,48	FOUR HUNDRED TWENTY-TWO EUROS AND FOURTY-EIGHT CENTS
4.3	u Exposition preparation	483,84	FOUR HUNDRED EIGHTY-THREE EUROS AND EIGHTY-FOUR CENTS

Table 5. Partial budget

ANNEXE JUSTIFICATION PRICES

Nº	Code	Ud	Description		Total
			1 Project definition		
1.1	01.01	**h**	**Meeting with thesis' tutors**		
	L.PHD	1,000 h	Thesis Professor Tutor	30,680	30,68
	L.IBE	1,000 h	Biomedical Engineering Student	9,640	9,64
	L.03	1,000 h	PhD thesis tutor	33,400	33,40
	L.04	1,000 h	Photonics Cathedratic thesis tutor	33,400	33,40

			Total price per h .		**107,12**

2 State of the art investigation

2.1 02.01	**u**	**State of the art**			
L.PHD		40,000 h	Thesis Professor Tutor	30,680	1.227,20
L.IBE		40,000 h	Biomedical Engineering Student	9,640	385,60
EQ.LO		40,000 h	Libre Office License	0,001	0,04
			Total price per u .		**1.612,84**

3 Methodology and results

3.1 03.01	**u**	**Theoretical sample design and microfabrication**			
L.PHD		1,000 h	Thesis Professor Tutor	30,680	30,68
L.IBE		1,000 h	Biomedical Engineering Student	9,640	9,64
EQ.ET		2,000 u	Etching: RIECIP	90,000	180,00
EQ.R		1,000 u	Coater EVG 101 (resin depositin)	50,000	50,00
EQ.PVA		3,000 u	Tepla PVA (resin depostition)	50,000	150,00
EQ.BM		1,000 u	Brewer Model (Aged and Developing)	50,000	50,00
EQ.LIT		1,000 u	Raith 150 (lithography)	500,000	500,00
EQ.Sim		3,000 h	CST STUDIO SUITE (simulation)	45,000	135,00
MAT.O		1,000 u	Wafer SOI	250,000	250,00
			Total price per u .		**1.355,32**

3.2 03.02	**u**	**BPT functionalization**			
L.PHD		5,000 h	Thesis Professor Tutor	30,680	153,40
L.IBE		5,000 h	Biomedical Engineering Student	9,640	48,20
MAT.H2O		1,000 L	MiliQ water	1,250	1,25
MAT.BPT		1,000 u	BPT (Biphenyl-4-thiol) Merck-Sigma Aldrich	44,500	44,50
MAT.B		1,000 u	Laboratory coat	15,000	15,00
MAT.CAMP		6,000 h	Exhaust hood	2,060	12,36

	MAT.ET	1,000 L	Ethanol	28,800	28,80
	MAT.G	1,000 u	Nitrile gloves	5,820	5,82
	MAT.TIP	3,000 u	Micropipette tips	11,500	34,50
	MAT.N2	11,000 m3	N2 stream	1,400	15,40
	MAT.mPIP	1,000 u	Micropipette 10-100 uL	310,510	310,51
	MAT.PI	1,000 u	Piranha solution	12,380	12,38
	MAT.CLAMP	1,000 u	Laboratory clamps	5,100	5,10
	EQ.US	0,083 h	Ultrasonic cleaner	45,000	3,74
			Total price per u .		**690,96**

3.3 03.03 **u** **Nanoparticle transfer by drop casting**

L.PHD	20,000 h	Thesis Professor Tutor	30,680	613,60
L.IBE	20,000 h	Biomedical Engineering Student	9,640	192,80
MAT.NP60	1,000 L	Gold nanoparticles 60 nm, 20 mL BBI SOLUTIONS	155,000	155,00
MAT.NP150	1,000 L	Gold nanoparticles 150 nm, 20 mL BBI SOLUTIONS	195,000	195,00
MAT.mPIP	1,000 u	Micropipette 10-100 uL	310,510	310,51
MAT.CLAMP	1,000 u	Laboraty clamps	5,100	5,10
MAT.H2O	1,000 L	MiliQ water	1,250	1,25
MAT.N2	11,000 m3	N2 stream	1,400	15,40
MAT.TIP	2,000 u	Micropipette tips	11,500	23,00
		Total price per u .		**1.511,66**

3.4 03.04 **u** **Nanoparticle transfer with PDMS**

MAT.NP150	1,000 L	Gold nanoparticles 150 nm, 20 mL BBI SOLUTIONS	195,000	195,00
MAT.mPIP	1,000 u	Micropipette 10-100 uL	310,510	310,51
MAT.CLAMP	1,000 u	Laboratory clamps	5,100	5,10
MAT.H2O	1,000 L	MiliQ water	1,250	1,25
MAT.N2	11,000 m3	N2 stream	1,400	15,40
MAT.TIP	2,000 u	Micropipette tips	11,500	23,00
MAT.NP60	1,000 L	Gold nanoparticles 60 nm, 20 mL BBI SOLUTIONS	155,000	155,00

	EQ.NPtransfer	1,000 h	NP set-up transfer	45,000	45,00
	MAT.PDMS	1,000 m3	Kit silicon Elastomer SYLGARD 184	170,000	170,00
	MAT.STC	1,000 u	Carbon conductive tape, double coated (TED PELLA, INC)	14,000	14,00
			Total price per u .		**934,26**
3.5 03.05	**u**	**Sample characterization**			
	MAT.CLAMP	1,000 u	Laboraty clamps	5,100	5,10
	L.IBE	40,000 h	Biomedical Engineering Student	9,640	385,60
	L.PHD	40,000 h	Thesis Professor Tutor	30,680	1.227,20
	EQ.RAs	60,000 h	Software Project 4.0 (Witec)	45,000	2.700,00
	EQ.RA	60,000 h	Spectroscopy alpha300 (Raman-AFM)	45,000	2.700,00
	EQ.DF	8,000 h	Dark Field Microscope	45,000	360,00
	MAT.STC	1,000 u	Carbon conductive tape, double coated (TED PELLA, INC)	14,000	14,00
	MAT.USB	1,000 u	USB Microscope	79,000	79,00
	EQ.SEM	5,000 h	Scanning electron microscope (SEM)	45,000	225,00
	MAT.AFM	2,000 u	AFM tips	50,000	100,00
			Total price per u .		**7.795,90**
3.6 03.06	**u**	**WERS set-up assembly**			
	L.IBE	40,000 h	Biomedical Engineering Student	9,640	385,60
	L.PHD	40,000 h	Thesis Professor Tutor	30,680	1.227,20
	EQ.LASER	20,000 u	Tunable semiconductor laser TSL-570 (1260nm - 1360 nm) SANTEC	45,000	900,00
	MAT.MICRO	1,000 u	Optical microscope	120,000	120,00
	MAT.USB	1,000 u	USB Microscope	79,000	79,00
	EQ.IR	20,000 h	Infrared camera XENICS	45,000	900,00
	EQ.SOURCE	20,000 h	Light source SCHOTT	45,000	900,00
	MAT.COLL	1,000 u	Collimator THORLABS	214,750	214,75
	EQ.MCAMERA	20,000 h	Camera adapted for use with microscope	45,000	900,00
	EQ.OSA	20,000 h	Optical signal analyzer HP HEWLLET PACKARD 26142A	45,000	900,00
	EQ.BOA	20,000 h	Booster optical amplifier THORLABS S9FC1132P	45,000	900,00

	EQ.VFL	20,000 h	Visual Fault Locator (YJ-250)	45,000	900,00
	MAT.P	1,000 u	Manual Fiber Polarization Controllers (ThorLabs)	323,370	323,37
	MAT.PW	1,000 h	Power meter	1.800,000	1.800,00
	EQ.ISO	20,000 h	Isolator (C00SS0021)	45,000	900,00
	EQ.BENCH	20,000 h	Optical bench	45,000	900,00
	MAT.OF	2,000 u	Optical fibre lensed	6,450	12,90
	MAT.MP	2,000 u	Machlift 60x60mm XYZ 3-Axis Linear Stage	119,000	238,00
	MAT.MP2	2,000 u	Machlifg LT60-LM XYZR 4-Axis LInear stage, rotation and goniometer	159,000	318,00
	EQ.3D	4,000 h	3d printer	45,000	180,00
	MAT.SNOM	1,000 u	NSOM probe 200 nm Cr-Au	1.598,500	1.598,50
	EQ.PCp	40,000 u	Personal computer	0,001	0,04
	MAT.OF_f	2,000 m	Fibre optic	0,600	1,20
			Total price per u .		**14.598,56**

4 Dissertation writing and correction

4.1 04.01	**u**	**Dissertation writing**			
	L.IBE	50,000 h	Biomedical Engineering Student	9,640	482,00
	EQ.LW10	50,000 h	Windows 10	0,001	0,05
	EQ.LO365	50,000 h	Office365	0,001	0,05
			Total price per u .		**482,10**
4.2 04.02	**u**	**Correction of the documents**			
	L.PHD	10,000 h	Thesis Professor Tutor	30,680	306,80
	L.IBE	12,000 h	Biomedical Engineering Student	9,640	115,68
			Total price per u .		**422,48**
4.3 04.03	**u**	**Exposition preparation**			
	L.PHD	12,000 h	Thesis Professor Tutor	30,680	368,16
	L.IBE	12,000 h	Biomedical Engineering Student	9,640	115,68

Table 6. Contractual implementation budget

Chapter		Import
1 Project definition .		214,24
2 State of the art investigation .		3.015,40
3 Methodology and results.		26.886,66
4 Thesis writing and correction.		1.388,42
Material execution budget		31.504,72
13% overheads		4.095,61
6% industrial profit		1.890,28
Suma	37.490,61	Suma
21% VAT		21% IVA
Contractual execution budget		45.363,64

5.3. COST OF AN INTEGRATED WERS PHOTONIC CHIP

As stated, the current work focuses on creating a WERS biosensor, whose objective is to develop a structure to measure waveguide Raman signal for biosensing applications. This can be also combined with the optical fibre integrated set-up assembled for measuring waveguide Raman signal. To provide an overview of how much one of these integrated sensors would cost, an economic analysis is presented in this section.

The estimated costs associated with each process and material are presented below:

- Silicon on insulator (SOI) 176.7 cm^2 wafer: 250 €
- PMMA resin deposition process, using *Coater EVG 101* and *Tecla PVA*, curing and revealing with *Brewer Model*: 150 €/wafer
- 5 hours *Ebeam* exposure: 2500 €
- Etching with *ICP-RIE*: 90 €/wafer
- BPT molecule: 44.5 €/ 25 g
- Accurate™ Spherical Gold Nanoparticles 60 nm: 100 €/25 ml
- Accurate™ Spherical Gold Nanoparticles 150 nm: 100 €/25 ml

The cots for one wafer in laboratory conditions would be 2945.5 €. Considering that an assembled chip measures 6 cm^2, and the wafer surface is 176.7 cm^2 it can be calculated the ratio 176.7 /6 = 29.45 chips. As the chips are squared and the wafer is round, we can approximate the

number of chips produce on a wafer would be 21 chips per wafer. This generates a manufacturing cost for a single chip 2945.5 €/21 chips = **140.27 €/chip under laboratory conditions**. Moreover, considering that per microchip would be used 10 µL of gold NPs, its price would be 0.01 ml × 4€/ml = 0.04 € = 4 cents. Thus, the price per chip assembled **under laboratory conditions amounts to 140.31 €/chip**. However, **considering mass production could reduce values to less than 1€/chip.**

REFERENCES

[1] Redolat, J., Camarena-Pérez, M., Griol, A., Kovylina, M., Xomalis, A., Baumberg, J. J., Martínez, A., & Pinilla-Cienfuegos, E. (2023). Accurate transfer of individual nanoparticles onto single photonic nanostructures. ACS Applied Materials & Interfaces, 15(2), 3558-3565. https://doi.org/10.1021/acsami.2c13633

[2] Wang, Zilong (2016) Waveguide Enhanced Raman Spectroscopy (WERS): principles, performance, and applications. University of Southampton, Doctoral Thesis, 171pp.

[3] Serebrennikova, K. V., Berlina, A. N., Sotnikov, D. V., Dzantiev, B. B., & Zherdev, A. V. (2021).

Raman scattering-based biosensing: New prospects and opportunities. *Biosensors, 11*(12) doi:10.3390/bios111205127

[4] C. V. Raman and K. S. Krishnan, "A new type of secondary Radiation," Nature, vol. 121, no. 3048, pp. 501–502, 1928

[5] Ettabib, M. A., Marti, A., Liu, Z., Bowden, B. M., Zervas, M. N., Bartlett, P. N., & Wilkinson, J. S. (2021). Waveguide enhanced raman spectroscopy for biosensing: A review. ACS Sensors, 6(6),

2025-2045. doi:10.1021/acssensors.1c00366

[6] Moskovits, M. (2005). Surface-enhanced raman spectroscopy: A brief retrospective. Journal of Raman Spectroscopy, 36(6-7), 485-496. doi:10.1002/jrs.1362

[7] Willets, K. A., & Van Duyne, R. P. (2007). Localized surface plasmon resonance spectroscopy and sensing. Annual Review of Physical Chemistry, 58(1), 267-297. https://doi.org/10.1146/annurev.physchem.58.032806.104607

[8] Walrafen, G. E.; Stone, J. Intensification of Spontaneous Raman Spectra by Use of Liquid Core

Optical Fibers. Appl. Spectrosc. 1972, 26 (6), 585−589

[9] Kanger, J. S.; Otto, C.; Greve, J. Stimulated Raman Gain Spectroscopy of Thin Layers Using Dielectric Waveguides. J. Phys. Chem. 1996, 100 (40), 16293−16297

[10] Vázquez-Lozano, J. E., Baumberg, J. J., & Martínez, A. (2022). Enhanced excitation and readout of plasmonic cavity modes in NPoM via SiN waveguides for on-chip SERS. Optics Express, 30(3), 4553. https://doi.org/10.1364/OE.446895

[11] Levy, Y.; Imbert, C.; Cipriani, J.; Racine, S.; Dupeyrat, R. Raman scattering of thin films as a

waveguide. Opt. Commun. 1974, 11 (1), 66−69

[12] Kanger, J. S., Otto, C., Slotboom, M., & Greve, J. (1996). Waveguide Raman spectroscopy of thin polymer layers and monolayers of biomolecules using high refractive index. Journal of Physical Chemistry, 100(8), 3288-3292. doi:10.1021/jp952566t

[13] Dhakal, A., Wuytens, P. C., Peyskens, F., Jans, K., Thomas, N. L., & Baets, R. (2016). Nanophotonic waveguide enhanced raman spectroscopy of biological submonolayers. ACS Photonics, 3(11), 2141-2149. doi:10.1021/acsphotonics.6b00593

[14] Kita, D. M.; Michon, J.; Hu, J. A packaged, fiber-coupled waveguide-enhanced Raman spectroscopic sensor. Opt. Express 2020, 28 (10), 14963

[15] Dhakal, A.; Subramanian, A. Z.; Wuytens, P.; Peyskens, F.; Le Thomas, N.; Baets, R. Evanescent excitation and collection of spontaneous Raman spectra using silicon nitride nanophotonic waveguides. Opt. Lett. 2014, 39 (13), 4025−4028.

[16] Ali Raza, Stéphane Clemmen, Pieter Wuytens, Michiel de Goede, Amy S. K. Tong, Nicolas Le

Thomas, Chengyu Liu, Jin Suntivich, Andre G. Skirtach, Sonia M. Garcia-Blanco, Daniel J. Blumenthal, James S. Wilkinson, and Roel Baets, "High index contrast photonic platforms for on-chip Raman spectroscopy," Opt. Express 27, 23067-23079 (2019)

[17] D. Kita, J. Michon, S. Johnson, and J. Hu, "Are slot and sub-wavelength grating waveguides better than strip waveguides for sensing?," Optica 5, 1046-1054 (2018).

[18] Lieber, Chad & Wu, Owen & Bergles, Eric & Qian, Jack & Chandler, Lin. (2012). Tissue Raman Measurement at 1064 nm. Spectroscopy -Springfield then Eugene then Duluth-. 15-15

[19] Zhao Y, Jenkins M, Measor P, Leake K, Liu S, Schmidt H, Hawkins AR. Hollow waveguides with low intrinsic photoluminescence fabricated with Ta(2)O(5) and SiO(2) films. Appl Phys Lett. 2011 Feb 28;98(9):91104. doi: 10.1063/1.3561749. Epub 2011 Mar 2. PMID: 21448254; PMCID: PMC3064680.

[20] Lee, W., Muñoz-Galindo, P., Hegeman, I., Yong, Y.-S., Dijkstra, M., García-Blanco, S. M., & Offerhaus, H. L. (2020). Study on multiple waveguide platforms for waveguide integrated Raman spectroscopy. OSA Continuum, 3(5), 1322. https://doi.org/10.1364/OSAC.389053

[21] Wuytens, P. C., Skirtach, A. G., & Baets, R. (2017). On-chip surface-enhanced Raman spectroscopy using nanosphere-lithography patterned antennas on silicon nitride waveguides. Optics Express, 25(11), 12926. https://doi.org/10.1364/OE.25.012926

[22] Coucheron, D. A., Wadduwage, D. N., Murugan, G. S., So, P. T. C., & Ahluwalia, B. S. (2019). Chip-based resonance raman spectroscopy using tantalum pentoxide waveguides. IEEE Photonics Technology Letters, 31(14), 1127-1130. https://doi.org/10.1109/LPT.2019.2915671

[23] Evans, C. C., Liu, C., & Suntivich, J. (2016). Tio 2 nanophotonic sensors for efficient integrated evanescent raman spectroscopy. ACS Photonics, 3(9), 1662-1669. https://doi.org/10.1021/acsphotonics.6b00314

[24] Castelló-Pedrero, L., Gómez-Gómez, M. I., Zurita, D., García-Rupérez, J., Griol, A., & Martínez, A. (2023). 1310 nm TM grating couplers to operate silicon nitride ring resonator biosensors. Results in Optics, 11, 100418. https://doi.org/10.1016/j.rio.2023.100418

[25] Castelló-Pedrero, L., Gómez-Gómez, M. I., García-Rupérez, J., Griol, A., & Martínez, A. (2021). Performance improvement of a silicon nitride ring resonator biosensor operated in the TM mode at 1310 nm. Biomedical Optics Express, 12(11), 7244. https://doi.org/10.1364/BOE.437823

[26] Espinosa-Soria, A., Pinilla-Cienfuegos, E., Díaz-Fernández, F. J., Griol, A., Martí, J., & Martínez, A. (2018). Coherent control of a plasmonic nanoantenna integrated on a silicon chip. ACS Photonics, 5(7), 2712-2717. https://doi.org/10.1021/acsphotonics.8b00447

[27] Baumberg, J. J., Aizpurua, J., Mikkelsen, M. H., & Smith, D. R. (2019). Extreme nanophotonics from ultrathin metallic gaps. Nature Materials, 18(7), 668-678. https://doi.org/10.1038/s41563-019-0290-y

[28] Jakob, L. A., Deacon, W. M., Arul, R., de Nijs, B., Mueller, N. S., & Baumberg, J. J. (2022). Accelerated molecular vibrational decay and suppressed electronic nonlinearities in plasmonic cavities through coherent raman scattering. https://doi.org/10.48550/ARXIV.2210.03569

[29] Chen, W., Roelli, P., Hu, H., Verlekar, S., Amirtharaj, S. P., Barreda, A. I., Kippenberg, T. J., Kovylina, M., Verhagen, E., Martínez, A., & Galland, C. (2021). Continuous-wave frequency upconversion with a molecular optomechanical nanocavity. Science, 374(6572), 1264-1267. https://doi.org/10.1126/science.abk3106

[30] Xomalis, A., Zheng, X., Chikkaraddy, R., Koczor-Benda, Z., Miele, E., Rosta, E., Vandenbosch, G. A. E., Martínez, A., & Baumberg, J. J. (2021). Detecting mid-infrared light by molecular frequency

upconversion in dual-wavelength nanoantennas. Science, 374(6572), 1268-1271. https://doi.org/10.1126/science.abk2593

[31] Wang, K., Mizuno, Y., Kishizawa, K., Toyoda, Y., Lee, H., Ichige, K., Kurz, W., Dong, X., Jakobi, M., & Koch, A. W. (2022). Temperature sensing based on multimode interference in polymer optical fibers: Sensitivity enhancement by PC-APC connections. Japanese Journal of Applied Physics, 61(11), 118001. https://doi.org/10.35848/1347-4065/ac9810

[32] Chiang, N., Scarabelli, L., Vinnacombe-Willson, G. A., Pérez, L. A., Dore, C., Mihi, A., Jonas, S. J., & Weiss, P. S. (2021). Large-scale soft-lithographic patterning of plasmonic nanoparticles. ACS Materials Letters, 3(3), 282-289. https://doi.org/10.1021/acsmaterialslett.0c00535

[33] Henzie, J., Lee, M. H., & Odom, T. W. (2007). Multiscale patterning of plasmonic metamaterials. Nature Nanotechnology, 2(9), 549-554. https://doi.org/10.1038/nnano.2007.252

[34] Mayer, K. M., & Hafner, J. H. (2011). Localized surface plasmon resonance sensors. Chemical Reviews, 111(6), 3828-3857. https://doi.org/10.1021/cr100313v

[35] Notingher, I. (2007). Raman spectroscopy cell-based biosensors. Sensors, 7(8), 1343-1358. https://doi.org/10.3390/s7081343

[36] Shafer-Peltier, K. E., Haynes, C. L., Glucksberg, M. R., & Van Duyne, R. P. (2003). Toward a glucose biosensor based on surface-enhanced raman scattering. Journal of the American Chemical Society, 125(2), 588-593. https://doi.org/10.1021/ja028255v

ANNEXE 1. OBJECTIVES OF SUSTAINABLE DEVELOPMENT(ODS)

Objectives of sustanaible development	High	Medium	Low	Not proceed
ODS 1. Poverty end.				x
ODS 2. Starvation end.				x
ODS 3. Health and wellbeing.	x			
ODS 4. Quality education.				x
ODS 5. Gender equality.				x
ODS 6. Clean water and safe sanitation.				x
ODS 7. Cleaner and affordable energy.				x
ODS 8. Decent work and economic growth.				x
ODS 9. Industry, innovation, and infrastructure.	x			
ODS 10. Inequality reduction.				x
ODS 11. Sustainable cities and communities.				x
ODS 12. Responsible production and consumption.				x
ODS 13. Climate action.				x
ODS 14. Submarine life.				x
ODS 15. Life of terrestrial ecosystems.				x
ODS 16. Peace, justice, and solids institutions.				x
ODS 17. Alliance to achieve objectives.				x

DESCRIPTION TO THE ALIGMNEMENT OF THE THESIS WITH THE ODS

ODS 3. Health and wellbeing

The current work focuses on the objectives of ODS 3, because of it is an investigation whose future applications can cause a severe impact in the national health system. ODS 3 points to some objectives coupled to the future applications of this work. First objective is the presence of COVID-19 sanitary crisis. Secondly, is the compromise with VIH/SIDA, malaria and other diseases. As this work is the first part of a future biosensor whose bioreceptor could be specific for anyone of those diseases. The development of a portable device will increase the detection process, rising the patient life quality. Furthermore, a fast and early detection of diseases will produce a faster treatment, a reduction of the waiting times and a higher number of diagnostics and treated patients.

ODS 9. Industry, innovation, and infrastructure.

The work realized in the thesis is based in the innovation of the Raman iteration biosensor, implementing the coupled electromagnetic beam using waveguides. The development of this kind of sensor will rise an industry and infrastructure associated to biomedical and telecommunications engineering. Creating the fundamentals for the development of a commercial device which will allows the resolution to real problems presents in the hospitals, the need of diagnostic diseases using a fast response method, simple and without the necessity of having a higher qualified professional.